Ore Geology Reviews 72 (2016) 232–252

Contents lists available at ScienceDirect

Ore Geology Reviews

journal homepage: www.elsevier.com/locate/oregeorev

Review

Unraveling rare earth element signatures in hydrothermal carbonate minerals using a source–sink system

David Debruyne *, Niels Hulsbosch, Philippe Muchez

KU Leuven, Department of Earth and Environmental Sciences, Celestijnenlaan 200E, B-3000 Leuven, Belgium

ARTICLE INFO

Article history:
Received 28 April 2015
Received in revised form 24 July 2015
Accepted 27 July 2015
Available online 29 July 2015

Keywords:
Rare earth elements
Hydrothermal
Fractionation
Carbonate minerals
Calcite
Dolomite

ABSTRACT

Rare earth element and yttrium (REEY) signatures in hydrothermal carbonate minerals are widely used proxies for studying hydrothermal mineralization. This review adopts a source–sink approach that synthesizes the current understanding of REEY mass transfer along the pathway of hydrothermal fluids. The merits of this process-centered approach are illustrated with representative examples, selected to disclose the interpretative possibilities and limitations of REEY studies on carbonates.

The starting points for the source–sink approach are the major fluid reservoirs: seawater, magmatic water and meteoric water. The REEY are subsequently added or removed during fluid–rock interaction by mineral breakdown, alteration and precipitation. These reactions largely determine redox conditions, pH and the element composition in the resulting fluids. Efficient complexation at high temperatures critically enhances REEY solubility in hydrothermal fluids, while sorption along the pathway becomes increasingly irrelevant at higher temperatures. Chlorine and fluorine are light REE (LREE)-selective ligands, while hydroxide and carbonate are heavy REE (HREE)-selective. These ligands can significantly fractionate the REE if they are major species. Fractionation occurs both by selectively increasing the transport capacity along the pathway and by preferentially retaining certain REE during precipitation. Comparison of mineral solubilities indicates that monazite generally limits the REEY content along the fluid pathway. Coprecipitating phosphates are expected to significantly diminish REEY availability for hydrothermal carbonates. Nonetheless, the trivalent REEY are highly compatible in the calcite lattice, especially LREE. The incorporation of REEY during calcite precipitation is relatively insensitive to kinetics, and can show significant concentration variations on small scales. Post-depositional interaction with calcite-undersaturated fluids preferentially removes the most fluid-mobile REEY from the unaltered precipitate, in the order: $Eu^{2+} >> LREE^{3+} >$ or $< HREE^{3+} >> Ce^{4+}$, with $Y^{3+} >$ or $\approx Ho^{3+}$, depending on the reaction conditions.

The main processes that determine REEY signatures in hydrothermal carbonate minerals are summarized in a number of flow charts that allow backtracking of their REEY characteristics along the fluid pathway. Application of this approach to some representative examples illustrates that pattern shape and anomalies can provide useful information on hydrothermal processes and conditions. The process-centered approach is especially useful in multiphase systems, where interpretation of pattern shape and Ce, Eu and Y anomalies can be ambiguous, even when abundant information from other methods is available. Presently, there is no consensus on an explanation for the commonly observed strong LREE depletion in hydrothermal carbonates compared to crustal reservoirs. We speculate that REEY solubility control by strongly LREE-selective phosphates such as monazite and by carbonates along the pathway significantly contributes to this strong LREE depletion. Ultimately, the observed pattern shape and anomalies are a function of many superimposed processes, all of which should be considered, taking into account the constraints provided by other methods.

Contents

* Corresponding author.
E-mail address: david.debruyne@ees.kuleuven.be (D. Debruyne).

http://dx.doi.org/10.1016/j.oregeorev.2015.07.022
0169-1368/

1. Introduction

The rare earth elements (REE) are a series of 15 lanthanoid elements that mostly form trivalent positive ions in hydrothermal fluids. Since the ionic radii decrease systematically across the lanthanide series, and certain ligands and minerals prefer smaller or larger ions, these ions are fractionated during hydrothermal transport. To a first approximation, this fractionation is governed by charge and radius controlled processes operating along the pathway of hydrothermal fluids (Möller, 1997). However, fractionation of the geochemical twins Y^{3+} and Ho^{3+} has shown that complexation with fluorine (Bau and Dulski, 1995), sorption to Fe–Mn oxyhydroxides (Bau and Dulski, 1999) and mineralogical control (Tanaka and Kawabe, 2006) can significantly fractionate ions with near-identical charge and radius in hydrothermal systems. In addition, cerium and europium can form tetravalent and divalent ions respectively, resulting in additional lanthanide fractionation, depending on redox state, temperature and pH of the system (Bau and Möller, 1992). The resulting REE and Y (REEY) composition of hydrothermal precipitates is therefore a suitable proxy to identify certain processes operating prior, during and post mineralization of hydrothermal deposits. Hydrothermal carbonates are commonly used for such studies, since they are nearly ubiquitous hydrothermal minerals and can easily accommodate REEY in their mineral lattice (Zhong and Mucci, 1995; Tanaka and Kawabe, 2006). However, backtracking of the effects of hydrothermal processes is complicated by limited constraints on the physicochemical conditions along the fluid pathway and superposition of different hydrothermal processes.

We adopt a source–sink approach to synthesize the current understanding of REEY mass transfer in hydrothermal systems, focusing on the effects of individual hydrothermal processes. This system conveniently describes mass transfer along the pathway from the source to the precipitation area. Major-fluid reservoirs like meteoric water, seawater and magmatic water are considered as a starting point in this system (Fig. 1). Along its pathway towards the studied hydrothermal precipitates, the fluid can equilibrate with different rock types at changing physicochemical conditions. During equilibration with solid reservoirs, REEY are acquired or removed through mineral breakdown, mineral alteration, sorption and precipitation of supersaturated minerals, modifying the composition of the fluids. At the same time, wall rock hydration, boiling and phase separation can also modify the fluid composition (Bodnar et al., 1985), while complexation significantly increases the fluid's REEY transport capacities (Haas et al., 1995), and can also fractionate REEY (Migdisov et al., 2009). When hydrothermal minerals are precipitated, the REEY are distributed along the coprecipitating mineral phases, while the fluid retains part of the REEY in solution (Bau and Möller, 1992). Finally, post-depositional remobilization can modify the REEY patterns.

The process-centered approach is then summarized in a number of flow charts and applied to four case studies to demonstrate that it constitutes a convenient framework to interpret REEY signatures, and can expose some limitations of their interpretative potential.

2. Normalization options: implicit assumptions and pitfalls

REEY patterns are often normalized over appropriate reference values and visualized in logarithmic plots, because order of magnitude differences in REEY concentrations are common in hydrothermal systems. Awareness of the differences between reference composition and the implicit assumptions associated with each of them is crucial to chose an appropriate reference composition and correctly interpret REEY data. The chosen reference compositions for hydrothermal precipitates are usually solid reservoirs, such as estimates of the upper crust composition or the primitive mantle composition (Fig. 2).

Normalization allows assessing the deviation from the chosen reservoir and has the additional benefit of removing the Oddo–Harkins effect, a see-saw pattern owing to the differential stability of nuclei with odd and even atomic numbers during nucleosynthesis. The bigger difference in radius between Nd and Sm, with atom numbers 60 and 62 respectively, generally results in a stronger fractionation compared to neighboring REE. Although promethium with atom number 61 is currently extinct, its inclusion in REEY plots is therefore highly recommended, since this emphasizes deviations from charge-and-radius-

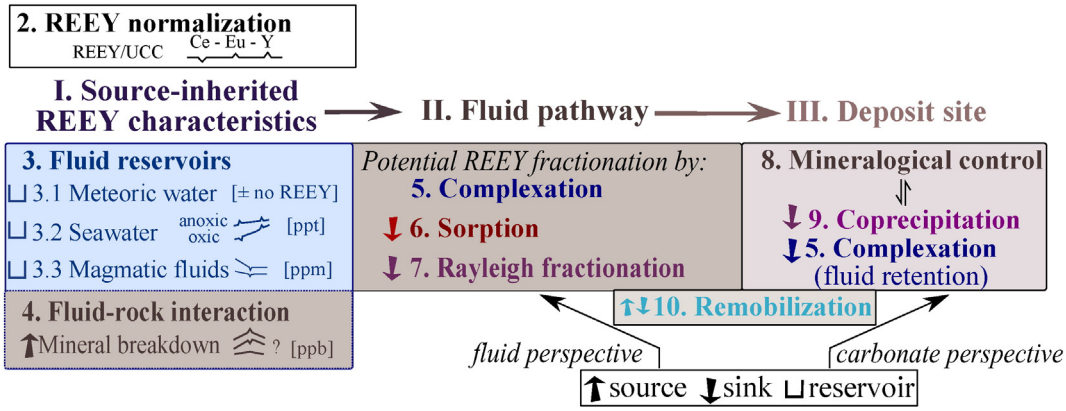

Fig. 1. Schematic diagram generalizing the hydrothermal REEY mass transfer in a source-sink framework, from (I.) the source-inherited features via (II.) the fluid pathway to (III.) the deposit site. The numbers indicated next to the reservoirs and the REEY fractionating processes correspond to the sections in the text. The shown patterns are normalized over UCC: Upper Continental Crust (Rudnick and Gao, 2003).

controlled behavior. Several commonly used reference compositions are shown in Fig. 2.

Compared to the Upper Continental Crust (UCC), normalization over Post-Archean Average Shale (PAAS) results in slightly lower LREE/$HREE_N$ ratios, slightly less pronounced HREE depletions and, most importantly, higher Eu/Eu_N^* values. The seawater composition is rarely used for normalization, although it is a sensible choice for marine carbonates, and could simplify interpretation considerably (e.g., Wang et al., 2014). The implicit assumption that the source area had a composition similar to the solid reference composition sometimes results in misleading concepts of REEY fractionation or anomalies. For instance, LREE enrichment in calcite with respect to the chondrite composition in crustal settings cannot be unequivocally attributed to calcite's LREE-selectivity if the composition of the parental fluids is not known. Moreover, the solid sources are likely LREE enriched compared to chondrite in crustal environments. This illustrates that the selection of the most appropriate reference values is best done in function of the specific research questions.

3. REEY inherited from major fluid reservoirs

3.1. Meteoric water

Initially, meteoric fluids are virtually devoid of dissolved ions, including REEY. As these fluids infiltrate sedimentary basins, meteoric waters incorporate REEY along with other ions, by dissolving undersaturated minerals. Since the REEY solubility is extremely low at ambient temperatures, mixing with meteoric water provides a potent precipitation mechanism (cf. Haas et al. (1995)).

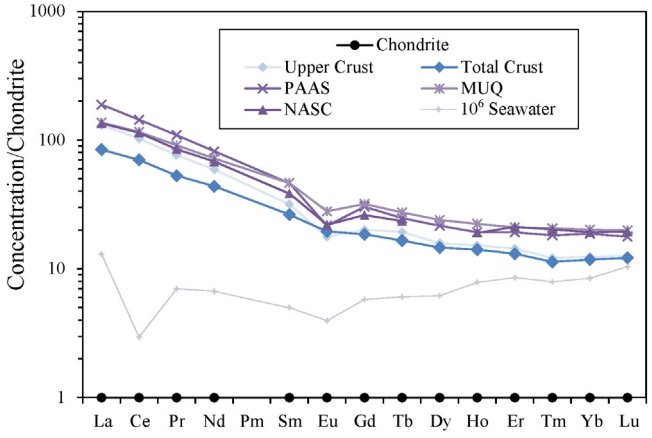

Fig. 2. Overview of commonly used REE reference compositions: Total and Upper Continental Crust (Rudnick and Gao, 2003), Post Archean Average Shale (PAAS; Pourmand et al., 2012), North American Shale Composition (NASC, Gromet et al., 1984), Mud of Queensland (MUQ; Kamber et al., 2005) and oxic Mediterranean seawater (Bau et al., 1997); normalized over the chondrite composition of Taylor and McLennan (1985).

3.2. Seawater

Seawater can be approximated as a H_2O–NaCl mixture, with minor SO_4, Mg, Ca, K and HCO_3 (Table 1; Turekian, 1968). Evaporation can easily increase the NaCl content from 3.5 to 25 wt.% before halite precipitates, even at ambient conditions. The presence of suitable ligands and interaction with the crustal rocks in a stationary equilibrium result in a REEY content that is orders of magnitude higher than in meteoric water, albeit still limited. Seawater typically contains ppt-levels of REEY, which is about 10^7–10^6 times lower than solid reservoirs (Fig. 3).

The marine REEY signature is characterized by a relative HREE enrichment when normalized over crustal reservoirs (Fig. 3). In addition, oxic seawater exhibits pronounced negative Ce anomalies, generated by Ce^{3+} sorption and subsequent, bacterially mediated oxidation (Moffett, 1990), or preferential sorption of tetravalent Ce to Fe- and Mn-oxides (Bau and Koschinsky, 2009). Similarly, the positive Y anomalies arise by conservative behavior compared to the lanthanoids during sorption to Fe–Mn oxides (Bau and Dulski, 1999). Seawater also has small positive La, Er and Gd anomalies when normalized over crustal compositions (e.g., Bau and Dulski, 1996; Kamber and Webb, 2001; Shields and Webb, 2004).

3.3. Magmatic fluids

The discrepancy in water content between saturated granite melts (4–8 wt.%) and solidified plutons (<1 wt.%), in combination with the size of typical granite plutons implies that enormous volumes of aqueous fluids are released during the crystallization (Petford et al., 2000; Thomas and Davidson, 2012; Yardley, 2013). Immiscible aqueous liquids are thus common in magmatic systems (cf. Veksler (2004)). In spite of their volumetric importance, little data is available about the REEY composition in natural aqueous fluids of magmatic origin, with the notable exception of Banks et al. (1994). High temperatures and ligand concentrations can easily result in ppm-level REEY concentrations in exsolved magmatic fluids. Experimental data indicates that aqueous fluids exsolving from monzogranites preferentially incorporate the LREE (Reed et al., 2000). The available REEY data on fluids with magmatic origin indicates a tendency towards LREE-enrichment compared to the crustal composition, sometimes with pronounced negative Eu anomalies (Fig. 4; Banks et al., 1994).

Table 1
Typical compositions for marine, crustal and magmatic aqueous fluids, including the main potential REEY ligands, expressed in ppm or wt. percentage (underlined).

Type	Seawater	Crustal fluids							Magmatic fluids					
T (°C)	−3 30	113	129	220	300	305	320	353	400	>600	450	>550	400	600
Na	1.08	1.79	2.98	4.57	6.22	5.3	5.46	0.96	17.9	19.6	13	7.8	1.63	3.95
K	392	140	230	0.71	1.46	1.67	1.16	0.15	6.1	7.5	9.3	3.7	0.42	1.45
Mg	0.129	117	151	128	0.12	33	639	<4	–	–	–	–	598	121
Ca	411	2.23	0.15	2.46	4.76	2.74	4.4	0.13	3.1	4.2	–	0.32	0.44	0.96
Sr	8.1	0.12	272	0.13	0.34	411	0.16	9	–	–	46	30	–	175
Fe	0.0034	–	–	0.24	0.29	0.16	2.38	56	–	–	17	6.0	0.91	1.2
Mn	0.0004	–	–	248	0.18	0.15	0.33	113	–	–	4.4	1.8	934	0.32
B	4.45	–	–	144	156	257	–	6	–	–	650	–	623	0.4
F	13	–	–	–	–	–	–	0.7	358	0.52	–	–	0.15	817
Cl	1.94	6.54	4.63	7.45	18.74	15.1	21.11	1.89	43	42.8	43	26.6	2.81	10.64
SO_4	0.27	2	18	887	0.22	65	0.12	–	2.1	2.4	–	–	0.21	0.61
H_2S	–	–	–		–	–	–	242	–	–	–	–	–	–
HCO_3	140	~61	~536	–	–	–	–	–	–	–	–	–	–	–
PO_4	0.27	–	–	–	–	–	–	–	–	–	–	–	–	–
Ref.	1	2	3	4	5	6	7	8	9		10		11	

References. 1: seawater (Turekian, 1968); 2, 3: thermal waters (Land and Macpherson, 1992); 4: Modum Complex, Norway (Munz et al., 1995); 5: Pyrenees (McCaig et al., 2000); 6: Salton Sea (Williams and McKibben, 1989); 7: Columbian emerald deposits (Banks et al., 2000); 8; Black Smoker Fluid (James et al., 2014), 9; Capitan Pluton (Banks et al., 1994); 10: Mole Granite (Audétat et al., 2000; Rankin and Ramsey, 1992); 11: Cornwall granite (Bottrell and Yardley, 1988).

4. Fluid–rock interaction

When fluids interact with solid reservoirs, their composition, redox state and pH are largely controlled by fluid–mineral equilibria, leaving temperature and chlorinity as the main independent variables (Hanor, 1994; Yardley and Bodnar, 2014). For convenience, we define crustal fluids here as fluids whose composition was significantly altered from the seawater, meteoric water or magmatic fluid composition by fluid–rock interactions. This section gives an overview of the effect of fluid–rock interactions on the fluid composition, REEY sourcing during fluid–rock interactions, and the imposed constraints on the redox state of certain REEY.

4.1. Fluid–mineral equilibria and physicochemical changes

Fluid–rock interaction has a strong influence on REEY behavior in hydrothermal systems, as it controls the availability of REEY-transporting ligands, and determines the availability of elements that constitute common carbonate minerals (Ca, Mg, Fe, Mn and CO_3). Most of these cations are major constituents in many crustal fluids, albeit less important than Na and K (Table 1). The abundance of Ca, Mg, Fe and Mn relative to the REEY in the fluid strongly influences the REEY content of hydrothermal carbonate minerals, but also the availability of CO_3 can limit the formation of carbonate minerals (e.g., Bau and Möller, 1992).

Because Mg is generally compatible during fluid–mineral interaction, many crustal fluids are relatively Mg-poor (Eugster and Gunter, 1981). Black smoker fluids are an example of seawater-derived, Mg-poor fluids that equilibrated with mafic oceanic crust (Table 1). Conversely, bittern brines that remain after NaCl deposition in evaporating seawater are strongly enriched in Mg (and K) compared to seawater (Carpenter et al., 1974). The concentration of transition metals such as Fe, Mn, Zn and Pb tends to increase as fluids interact with rocks at increasing temperature and chlorinity (Yardley, 2013).

Crustal fluids are enriched in Ca compared to evaporated seawater of similar chlorinity (McCaffrey et al., 1987), except when they equilibrate with Ca-poor systems, such as evolved granites. Calcium enrichment mainly occurs by albitization of plagioclase or through interaction with carbonates, e.g., by dolomitization (Carpenter et al., 1974; Heijlen et al., 2001; Warren, 2006). Most naturally abundant anions form insoluble minerals with Ca such as fluorite (CaF_2), calcite ($CaCO_3$), anhydrite ($CaSO_4$) and apatite ($Ca_5(PO_4)_3$ (OH, F, Cl)). Consequently, Ca-release during fluid–rock interaction generally decreases the concentrations of these anions, and the fluid's anion content tends to approximate the chlorinity (Yardley and Bodnar, 2014).

Carbon dioxide can be added to a fluid by decarbonation of carbonates (Eugster, 1981). It combines with water to form the carbonate anion and is completely soluble in pure H_2O at temperatures above ~250 °C. However, NaCl commonly present in hydrothermal fluids inhibits H_2O–CO_2 mixing and extends immiscibility to higher temperatures and pressures (Diamond, 2003). The presence of an immiscible CO_2 phase also constrains the fluid's pH, because of equilibrium reactions involving CO_3, HCO_3 and H_2CO_3, thereby governing the availability of OH for REEY complexation.

4.2. REEY sourcing during fluid–rock interactions

The addition of REEY during fluid–rock interaction is one of the most elusive concepts in hydrothermal systems. As hydrothermal fluids move through the subsurface towards the deposition site, all interacting rocks along their pathway can source or remove REEY. In most cases, fluids with continuously evolving compositions interact with different

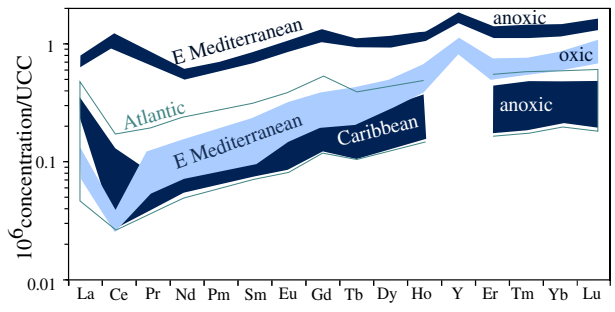

Fig. 3. Upper Continental Crust (UCC)-normalized REEY data from several ocean basins. Data from De Baar et al. (1985) and Bau et al. (1997).

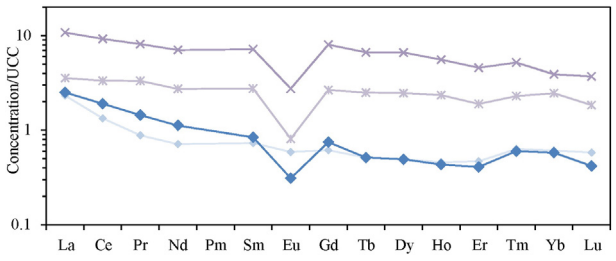

Fig. 4. REEY content in magmatic fluid inclusions from the Capitan pluton (Banks et al., 1994), normalized over the Upper Continental Crust (UCC).

rock types along their pathway, at varying pressure and temperatures. During fluid–rock interaction, dissolution of REEY-sourcing minerals is likely incongruent, and different minerals have different susceptibilities at the prevailing reaction conditions (Möller and Giese, 1997). Equilibration between the fluid and the available rock surface eventually results in a depleted zone or generates alteration products which form a protecting layer (Möller and Giese, 1997).

Solubility studies can serve as a first approximation for the reactive REEY composition of polymineralic REE sources. Theoretically, leaching studies of representative polymineralic systems at a range of hydrothermal conditions would provide empirical constraints on silicate sourcing behavior. In practice, this is difficult to achieve and leaching studies measuring REEY release are relatively rare.

The easily accessible REEY content was determined for a number of granites, gneisses and low-grade metasedimentary samples using a cation exchange resin to extract REEY at 70 °C and pH ~ 3 (e.g., Möller et al., 1997a, 1997b, 2003, 2004). This generally resulted in upward-convex crust-normalized REEY patterns (Fig. 5). Similar patterns were also obtained with HCl and acetate leaching of sediments (Ohr et al., 1994), who suggested that such patterns are dominantly generated by apatite breakdown. The refractory nature of the HREE can be attributed to their containment in stable mineral phases, such as zircon (e.g., Lüders et al., 1993). Granite leachates generally show higher yields for HREE than LREE, with an abrupt increase at Sm (e.g., Möller et al., 1997b). Compared to fresh granites, weathered granites have higher yields for the HREE and similar to lower yields for the LREE, suggesting that the LREE are redistributed in more stable phases during weathering (Möller 2002). The Nd–Sm fractionation between leachates and whole rock appears to be more pronounced for granites than for metasedimentary samples (Fig. 5). Moreover, the results from Möller et al. (1997b) also indicate that Y and Ho are not significantly fractionated during leaching. Leaching experiments on basalts at ambient conditions resulted in elemental yields that were inversely proportional to their partitioning ratio in the leached minerals (Shibata et al., 2006). This implies that bulk partition coefficients provide a first approximation for the yield of polymineralic systems.

Reproducing the reactive source composition requires extensive knowledge of conditions, kinetics and mineral stabilities in complex polymineralic systems along the fluid pathway. For this reason, the aforementioned experiments are likely not representative for hydrothermal leaching conditions. Nonetheless, these experiments can give an indication of the expected REEY release by crustal rocks.

4.3. REEY redox reactions in crustal fluids

When fluids interact with the surrounding solid reservoirs, the reduction potential (Eh) is governed by mineral redox buffers such as the hematite–magnetite buffer (Fig. 6). Since oxidized species of Fe and Mn are fluid-immobile, S and C species are likely the main mobile redox agents in fluids and redox reactions with H_2O are common (e.g., Yardley and Bodnar, 2014). In natural aqueous environments REE redox reactions are limited to Eu and Ce (Bau and Möller, 1992). Significant Yb anomalies are not known in hydrothermal deposits, placing a lower bound on $fO_2(T)$ in hydrothermal environments (Fig. 6; Bau and Möller, 1992). The redox reactions are dependent on temperature, pH, REEY speciation and pressure. Bau and Möller (1992) wrote the redox reactions for Eu as alkaline (1) and Ce in acidic (4) reactions respectively, but their corresponding reactions can also be considered:

$$2Eu^{3+}2OH^- = 2Eu^{2+} + H_2O + 0.5O_2 \quad (1)$$

$$2Eu^{3+} + H_2O = 2Eu^{2+} + 2H^+ + 0.5O_2 \quad (2)$$

$$2Ce^{3+} + 6OH^- + 0.5O_2 = 2CeO_2 + 3H_2O \quad (3)$$

$$2Ce^{3+} + 3H_2O + 0.5O_2 = 2CeO_2 + 6H^+ \quad (4)$$

The aforementioned reactions show that both redox reactions have a strong pH dependence, especially Ce oxidation. Nonetheless, tetravalent Ce is generally limited to oxidizing sub-aerial environments (Bau and Möller, 1992). When the oxygen fugacity is buffered by hematite–magnetite, Eu^{3+} is thermochemically reduced at temperatures above ~200 °C (Fig. 6; Bau and Möller, 1992). Higher pH values reduce the stability fields of Ce^{4+} and Eu^{2+}, implying that the reduction of Eu occurs at higher temperatures. At temperatures above 250 °C, Eu^{2+} is

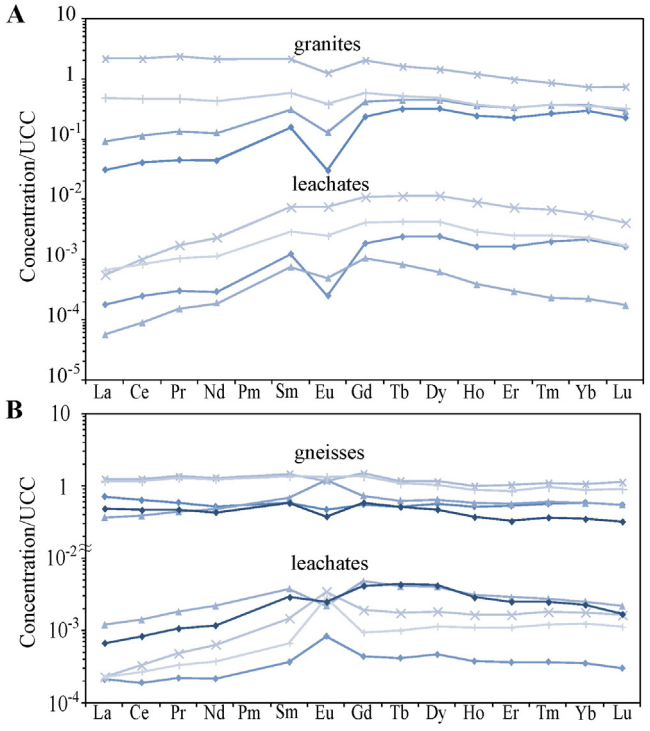

Fig. 5. Leaching experiments with cation exchange resin at 70 °C showing the easily accessible REE content of several granites and gneisses as representative magmatic and high-grade metamorphic sedimentary rocks respectively. The granite leachates display a more pronounced Sm–Nd fractionation compared to the gneisses. Data from Möller et al. (1997b).

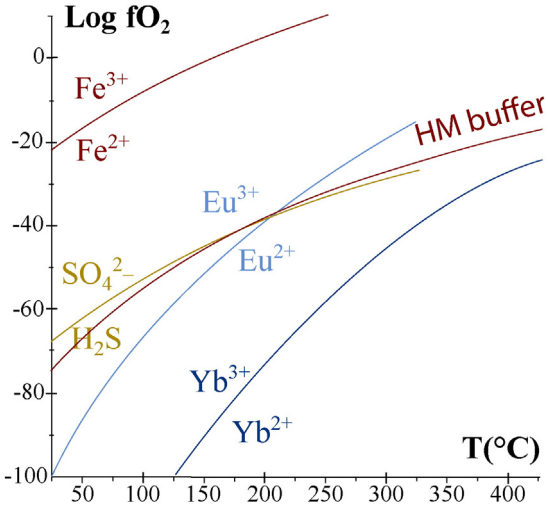

Fig. 6. Calculated redox equilibria at pH 3 for the hematite–magnetite oxygen fugacity (HM) buffer, Fe^{2+}/Fe^{3+}, Eu^{2+}/Eu^{3+} and H_2S–SO_4 at 50 MPa and for Yb^{2+}/Yb^{3+} at 100 MPa. Modified from Bau and Möller (1992).

expected to dominate in aqueous fluids (Sverjensky, 1984). Importantly, Eu anomalies generated in hydrothermal conditions can be preserved in low-temperature precipitates wherein Eu is trivalent (Bau et al., 2010).

Eu and Ce anomalies are commonly expressed in the following form:

$$\frac{Eu_N}{Eu_{N^*}} = \frac{Eu_N}{0.5(Sm_N + Gd_N)} \quad (5)$$

$$\frac{Ce_N}{Ce_{N^*}} = \frac{Ce_N}{0.5(La_N + Pr_N)} \quad (6)$$

The subscript N indicates the normalization over the chosen reference values. Eu* and Ce* are the expected concentration based on the interpolation between the concentrations of the neighboring REE. Ratios (5) and (6) above and below unity are termed positive and negative anomalies, respectively. Ce anomalies in hydrothermal precipitates are either inherited from marine waters or generated during post-depositional remobilization at near-surface conditions (Bau and Dulski, 1996). In such conditions, Eu is normally trivalent, and therefore Eu and Ce cannot be generated simultaneously (Bau and Möller, 1992). Backwards extrapolation from Sm, Nd and Pr reveals anomalously high La concentrations in modern seawater (e.g., Bau and Dulski, 1996). Such positive La anomalies result in 'apparent' negative Ce anomalies using Eq. (6). Bau and Dulski (1996) designed the Ce/Ce*–Pr/Pr* plot to resolve this. This plot can distinguish between La and Ce anomalies, since Pr*, interpolated between Ce and Nd, is only affected by anomalous Ce concentrations.

5. Complexation

5.1. REEY transport capacity increases

At ambient temperatures, lanthanide ions form complexes with the dipolar water molecules, generating a hydration sphere. These hydration spheres shield the lanthanides from complexing with anionic species and free aqueous species dominate, reducing complexation with stronger ligands (Haas et al., 1995). Nonetheless, strong REEY ligands such as CO_3^{2-} and PO_4^{3-} can dominate REEY speciation when these are abundant, for instance in seawater (e.g., Haas et al., 1995; Lee and Byrne, 1992).

With increasing temperature, hydration becomes energetically less favorable, the coordination number of aquo-complexes decreases and shielding by aqueous ligands is consequently less effective (e.g., Haas et al., 1995; van Sijl et al., 2009). Complexation with anionic ligands then results in progressively higher REEY solubilities (e.g., Haas et al., 1995). The hard–soft acid–base principles of Pearson (1963) predict that the small, highly charged REE^{3+} ions form strong bonds with hard ligands such as OH^-, F^-, CO_3^{2-} and SO_4^{2-}, thereby replacing one or more H_2O molecules in the hydration sphere. Stable complexes also have low solubilities (Pearson, 1963), which limits their transport capacities. In the context of hydrothermal REEY deposits, this favors ligands with intermediate bond strengths, such as Cl (Migdisov and Williams-Jones, 2014). Furthermore, hard ligands are sometimes not completely dissociated at low pH conditions in some natural systems, further reducing their availability for REEY complexation.

Experimental results at ambient conditions were extrapolated to hydrothermal or magmatic conditions up to 0.5 GPa and 1000 °C using the revised Helgeson Kirkham Flower (HKF) equation (Haas et al., 1995; Wood, 1990b). Their results confirm that the temperature increase causes a significant increase in stability constants with most hard ligands (e.g., OH^-, CO_3^{2-}, PO_4^{3-} and SO_4^{2-}), counteracted by a less pronounced effect from the pressure increase. Speciation is also strongly pH dependent and hydroxide complexes tend to dominate in alkaline conditions. Moreover, weak acids like HF, H_2CO_3, H_3PO_4 and H_2SO_4 are not significantly dissociated at acid conditions, with profound implications for REE transport.

Furthermore, experimental studies indicate that earlier HKF-based extrapolations overestimate the stability of the F and OH complexes and underestimate the increase in stability of the SO_4 complexes at higher temperatures (Migdisov and Williams-Jones, 2007; Migdisov et al., 2008, 2009; Wood et al., 2002). Although REE-F species are still three to four orders of magnitude more stable than REE-Cl at hydrothermal conditions, they are insoluble over a wide pH range, decreasing their potential as REE mobilizing ligands (Migdisov and Williams-Jones, 2014; Williams-Jones et al., 2012). Hydroxides also form extremely stable but insoluble complexes with REE at typical hydrothermal conditions (Migdisov and Williams-Jones, 2014). Nonetheless, speciation calculations indicate that REE-hydroxide species can dominate, even in fluids with pH as low as 3 (e.g., Pourtier et al., 2010). Carbonate and phosphate are expected to form stable, insoluble complexes with the REE at hydrothermal conditions (Haas et al., 1995; Wood, 1990b). The extremely low solubility of REE-PO_4 minerals is thought to limit the REE content in the fluid (Poitrasson et al., 2004; Wood, 2004; see Section 8), while the hydrothermal behavior of REE-carbonate species is not yet verified experimentally at this moment.

Recent experimental studies show that the REE form unexpectedly strong complexes with Cl, a ligand of intermediate strength (e.g., Gammons, 1996; Migdisov and Williams-Jones, 2002). Moreover, chlorine is by far the most abundant anion in many hydrothermal systems (Table 1). Consequently, speciation calculations for ocean-floor vents indicate that REE-Cl species dominate, even if the underestimated stability constants are used (e.g., Bach et al., 2003; Douville et al., 1999). Furthermore, the strong acid HCl is fully dissociated at low pH and REE-Cl complexes are highly soluble. Therefore, Cl is likely the main REEY transporting ligand in REEY ore-forming hydrothermal systems (e.g., Haas et al., 1995), although SO_4 and F can be important too (Migdisov and Williams-Jones, 2014).

Differences between experimental and theoretical values may result in solubility estimates varying over orders of magnitude (Table 2; Poitrasson et al., 2004). This illustrates that REEY speciation is highly sensitive to the values of the stability constants and highlights the necessity for an accurate experimental framework of stability constants to further calibrate thermodynamic parameters and allow speciation calculations for each specific hydrothermal environment.

5.2. Complexation-driven REEY fractionation

The lanthanide–ligand interactions are mostly ionic with a minor covalent component (e.g., Adamo and Maldivi, 1997) and thus follow Coulomb's law. The electrostatic attraction is thus proportional to the charge of ions and inversely proportional to the ionic radius squared. Both Coulomb's law and density functional theory (DFT) computations predict higher stability of complexes with the smaller HREE ions, both at ambient and at high pressures–high temperature conditions (e.g., van Sijl et al., 2009). These calculations also indicate that the strength of the lanthanide–ligand bond and its length vary with the geometry and coordination number of hydration sphere. This geometry is different across the lanthanide series and the coordination numbers decrease with increasing temperatures (van Sijl et al., 2009).

At ambient conditions, the largest lanthanides (La–Nd) are dominantly hydrated by 9 H_2O molecules arranged as tri-capped trigonal prisms. Ions smaller than Sm are then surrounded by 8 H_2O molecules in square antiprismatic structures, while Sm and Gd exhibit intermediate behavior (Van Sijl et al., 2009). This study illustrates the crucial role of the local environment during complexation. For instance, the dielectric constant of a solvent, a measure for the long-range perturbation of the solvent by charged species, may be insufficient to explain complexation systematics (van Sijl et al., 2009). In practical terms, this implies that activity models based on a bulk property like a dielectric constant,

Table 2
Overview of the currently available stability constants for La, Nd and Lu complexes at ambient and hydrothermal conditions. Species that tend to be most prominent for each ligand are in bold.

Ligand	β_x	25 °C, 1 atm		300 °C, P_{sat}				
		EXP		HKF		EXP		
		La	Lu	La	Lu	La	Nd	Lu
OH^- (2)	β_1	5.34	6.41	9.5	10		8.2	
	β_2	**9.86**	**12.65**	**16**	**17.5**		**14.5**	
	β_3	**14.09**	**18.14**	**23**	**25**		**20.4**	
	β_4	15.14	24.05	26	30			
F^-	**β_1**	**3.85**	**4.83**	**8**	**9**	**8.18**	**8.08**	**6.85**
	β_2	6.65	8.44	12	14	–		
	β_3	8.69	11.10	13	15	–		
	β_4	10.35	13.29	9	12	–		
Cl^- (2)	**β_1**	**0.29**	**−0.03**	**4**		**4.59**	**4.75**	**2.71**
	β_2	**−0.03**	**−0.62**	**5.5**		**6.61**	**5.87**	**5.16**
	β_3	−0.41	−1.20	4		–		
	β_4	−0.83	−1.79	1.5	0	–		
HCO_3^- (2)	β_1	2.02	1.90	3.5	3	–		
CO_3^{2-}(1)	β_1	7.12	8.29	8.75		–		
SO_4^{2-} (3)	**β_1**	**3.62**	**3.59**	**7.7**	**7.9**		**≈HKF**	
	β_2	1.67	1.79	4.98	2.63		≈HKF	
$H_2PO_4^-$ (2)	β_1	2.5	2.3	4		–		
NO_3^{2-} (2)	β_1	≈0.6		≈0.5		–		

Experimental β_1 at 25 °C from (1) Lee and Byrne (1992), (2) Millero (1992) and (3) Powell (1974). Experimental HKF stability constants and β_2–β_4 by Haas et al. (1995); β_2 SO_4 from Wood (1990a). Experimental Nd hydrolysis at 290 °C, P_{sat} from Wood et al. (2002) and the K_w values from Verma (2003). Experimental Cl and F stability constants extrapolated from experimental data (≤250 °C) using revised HKF parameters by Migdisov et al. (2009), experimental SO_4 results fromMigdisov et al. (2008).

such as the (extended) Debeye–Hückel equation, the Pitzer equations, and the HKF model may not be fully adequate.

The theoretical extrapolations from Haas et al. (1995) indicate that hydroxides have a relatively small preference for HREE, but this has not been confirmed experimentally. The available theoretical and experimental framework suggests that sulfate complexes have no major preference for either LREE or HREE (Schijf and Byrne, 2004). Carbonate complexes are strongly HREE selective at ambient conditions (Lee and Byrne, 1992), and this tendency persists at higher temperatures (Tsay et al., 2014). Similarly, the theoretically predicted HREE-preference from fluorides (e.g., Haas et al., 1995) is contradicted by experimental studies, which indicate that LREE-F complexes are significantly more stable than HREE-F complexes (Migdisov et al., 2009). Certain hydrothermal vents (Douville et al., 1999) and experimental fluids (Allen and Seyfried, 2005) suggested LREE-selectivity for chloride. However, no LREE-selectivity was predicted (Haas et al., 1995) and speciation studies did not demonstrate any LREE preference within the experimental uncertainties (Gammons, 1996). However, more recent speciation studies confirmed a LREE-preference for chloride, provoking a change of REEY parameters in the HKF model (Mayanovic et al., 2009; Migdisov et al., 2009).

The LREE preference from Cl and F indicates that the increasing strength of the ionic bond for ions with smaller radii is counteracted by a stronger effect. Synchrotron X-ray absorption spectrometry suggests that this is due to steric hindrance, i.e., spatial hindrance from other atoms or electron clouds (Mayanovic et al., 2009). In combination with lanthanide contraction, steric hindrance causes a reduction in chloride coordination of REE^{3+}-chloroaquo complexes from LREE to HREE (e.g., Mayanovic et al., 2009). The presence or absence of steric hindrance for the smaller F ligand has not yet been investigated. Although the steric hindrance can account for the higher LREE coordination numbers, it does not explain the increased stability constant for the first complex (cf. Migdisov et al. (2009)).

At ambient conditions, the experimentally determined stability of mono-fluoro complexes decreases from Y ≈ Lu > Ho > La (Walker and Choppin, 1967). Such complexation-driven REE-Y fractionation is confirmed for natural fluorites precipitating from medium temperature (100–185 °C) hydrothermal fluids, which have elevated Y/Ho mass ratios around 75, up to 200 (Bau and Dulski, 1995). Since Y is equally mobile as its geochemical twin Ho during silicate leaching experiments, these Y/Ho anomalies are acquired during complexation-driven fractionation (Bau and Dulski, 1995; Möller et al., 1997a). Although Y–Ho ratios are often elevated in hydrothermal calcites, extremely high ratios are usually not observed, even where the total REE content correlates with the F concentrations in fluid inclusions (Kučera et al., 2009).

Divalent Eu has a radius comparable to Sr^{2+} (Shannon, 1976), indicating a high aqueous solubility. Moreover, hydrothermal fluids reacting with peridotites at 400 °C and 0.5 GPa acquire pronounced positive Eu anomalies upon Cl addition (Allen and Seyfried, 2005). This indicates that Cl addition significantly increases Eu^{2+} solubility, implying that it forms significantly more stable complexes with Cl relative to the trivalent REEY. This confirms the theoretical predictions from Haas et al. (1995), and implies that complexation-driven fractionation is the main factor generating pronounced positive Eu anomalies in ocean-floor hydrothermal vent fluids (e.g., Craddock et al., 2010).

6. Sorption

6.1. Sorption along the pathway: REEY sink?

Surface complexation, better known as sorption decreases the fluids REEY content as sorbed ions are lost from the fluid. Because sorption decreases with increasing temperature, complexation is expected to prevail at high-temperature hydrothermal conditions (Bau, 1991). Even at lower temperatures, sorption is strongly modified by complexation, because REEY have strong tendencies to form complexes (e.g., Haas et al., 1995). For instance, sorption at ambient conditions is governed by the presence of carbonate complexes (e.g., Byrne and Kim, 1990; Quinn et al., 2006a, 2006b). Adding low amounts of carbonates results in a sorption of REEY-CO_3^+ complexes in addition to M^{3+} species. At higher carbonate concentrations, sorption decreases due to REEY retention in the fluid by carbonate complexes. REEY sorption in natural systems is difficult to quantify due to the mineralogical complexity of natural rocks (e.g., Tertre et al., 2008). Moreover, sorption depends on mutually dependent parameters such as sorption site density, sorbent speciation and the mineral surface potential (Tertre et al., 2008). Sorption experiments at ambient conditions show that sorption increases strongly with decreasing ionic strength between 0.5 and 0.025 M (Tertre et al., 2008).

6.2. Sorption effects on REEY fractionation

Like complexation, sorption is mostly an electrostatic process governed by Coulomb's law and is expected to be more efficient for the smaller heavy REE. This would then result in LREE enrichment in sorption-dominated systems, while HREE enrichment is expected in complexation-dominated systems (Bau, 1991). Experimentally, sorption to various surfaces generally resulted in HREE enrichments in seawater-like fluids, and this was attributed to complexation-driven fractionation (e.g., Byrne and Kim, 1990). When this complexation-driven fractionation was taken into account, sorption by iron oxides at a wide range of pH (4–9) and ionic strength (0–0.7 M) conditions indicate no significant preference for either LREE or HREE in absence of complexation-driven fractionation (Quinn et al., 2006b). These results suggest that REE^{3+} fractionation by fluid complexes tends to dominate fractionation by surface complexation.

Experimental results in NaCl–H_2O system confirm a strong influence of complexation on sorption behavior (Jordan et al., 2011). They attribute a linearly increasing absorption free energy with increasing atom number to the increasing covalent binding properties for the HREE (e.g., Adamo and Maldivi, 1997). The latter resulted in a larger proportion of M–Cl complexes at these ambient conditions. Sorption of these M–Cl complexes then increases sorption efficiency. The combined effect

of sorption and complexation generally results in increasing HREE/LREE and Y/Ho ratios in ambient and hydrothermal seawater (e.g., Möller et al., 1991).

7. Rayleigh fractionation of minerals

Except for chloride, the main hydrothermal REEY ligands (F, CO_3, PO_4 and SO_4) form relatively insoluble compounds, thus limiting the fluid's REEY transport capabilities (e.g., Williams-Jones et al., 2012). Apart from some REEY ore-forming LREE rich hydrothermal systems (e.g., Smith et al., 2000), LREE-depleted signatures appear to be common in many hydrothermal systems and suggest Rayleigh fractionation of a LREE-selective mineral (e.g., Bau and Möller, 1992). The LREE-selective monazite (REE-PO_4) has the lowest solubility product of all simple REEY compounds in pure water (Poitrasson et al., 2004; Yurimoto et al., 1990). Since monazite is a common mineral in the upper crust, it likely limits REEY concentrations in many hydrothermal systems (Byrne and Kim, 1993; Poitrasson et al., 2004; Wood, 2004).

Monazite solubility has been studied in $H_2O \pm$ NaCl fluids at conditions ranging from hydrothermal to high pressure-high temperature conditions characteristic for subduction zones (Table 3). Monazite dissolution is retrograde in acid fluids between 21 and 300 °C, as a result of displacement of the solubility curve towards lower pH with increasing temperature (Poitrasson et al., 2004). In neutral to alkaline $H_2O \pm$ NaCl fluids between 21 and 800 °C, solubility is prograde and temperature increase has a strong positive effect on monazite solubility (Pourtier et al., 2010), while pressure increase has a relatively weak positive effect (Gibert and Montel, 1996; Pourtier et al., 2010). Tropper et al. (2011) found that NaCl addition increases monazite solubility to a much larger extent than pressure, where REE-chlorides are major species. This effect was much stronger for Ce (factor 223 at 0.5 X_{NaCl}) than for Y (factor 18 at 0.5 X_{NaCl}), where increasing Na yielded diminishing returns. This was attributed to mixed complexation with OH and Cl for the HREE and is consistent with the higher stability constants of the LREE-Cl complexes (e.g., Migdisov et al., 2009). However, Pourtier et al. (2010) observe no effect of NaCl addition and infer that REE-Cl complexes are negligible at their experimental conditions. The experiments from Pourtier et al. (2010) in turn indicate that extrapolations of experiments at pH 2 (Poitrasson et al., 2004) underestimate monazite solubility in the higher pH range. High monazite solubility at neutral to alkaline pH is confirmed at higher temperatures and pressures (800 °C, 1 GPa; Tropper et al., 2011). Possible reasons for the discrepancies between the experimental studies are discussed in depth by Pourtier et al. (2010). From this discussion, it is clear that the discrepancies between the experimental studies are largely related to the uncertainties associated with the speciation calculations, phosphate species in particular, and activity models.

8. Mineralogical control by carbonates

The two most common carbonates, calcite ($CaCO_3$) and dolomite ($CaMg(CO_3)_2$) form 'gangue minerals' associated with a variety of hydrothermal ore minerals and commonly incorporate trace amounts of REE. Consequently, carbonates are among the most widely studied REEY repositories (e.g., Banner et al., 1988; Bau and Möller, 1992; Wagner et al., 2010). Experimental partitioning data is only available for calcite. Therefore, this section first discusses the factors controlling REEY uptake by calcite, before summarizing the current state of knowledge of mineralogical control by other carbonate minerals.

8.1. REEY partitioning

Calcite precipitates from the fluid according to reactions (7) and (8) (Bau and Möller, 1992). These reactions illustrate that calcite precipitation increases the solubility of calcite by H^+-production, implying incremental calcite precipitation (Bau and Möller, 1992).

$$Ca^{2+} + CO_2 + H_2O \rightleftharpoons CaCO_3 + 2H^+ \quad \text{(open system, } CO_2 \text{ replenished)} \tag{7}$$

$$Ca^{2+} + HCO_3^- \rightleftharpoons CaCO_3 + H^+ \quad \text{(closed system)} \tag{8}$$

The partitioning of trace elements in minerals precipitating from a fluid is governed by Eq. (9) (Doerner and Hoskins, 1925). However, experimental results show that REEY coprecipitation decreases with increasing ligand concentration (Matsui, 1966). This indicates that only free ions or weakly complexated REEY are coprecipitated (Bau and Möller, 1992; Terakado and Masuda, 1988). If the REEY in the fluids form stable complexes $REEX_j$, the Doerner–Hoskins equation can then be written as (Bau and Möller, 1992):

$$\frac{d(REEY_i)}{d(Ca)} = \frac{L_0\left([REEY_i] \Big/ \left(1 + \sum K_{ij}[X]^j\right)\right)}{[Ca^{2+}]} \tag{9}$$

Where L_0 is the distribution ratio for the i-th REEY element that is considered (La, Pr,…, Lu) and $K_{ij}[X^j]$ is the product between the stability constants this element and the concentration of free anions j $[X^j]$. Dividing by factor $(1 + \sum K_{ij}[X^j])$ adjusts the total concentration of the element $[REEY_i]$, so that only free or weakly bound species are taken into account. When complexes have differential stability for light and heavy REE, this can lead to REEY fractionation. For instance, when [Ca] is the limiting factor during calcite precipitation, the precipitating calcite will be depleted in HREE with respect to the fluid (Bau and Möller, 1992). Because it is impractical to obtain instantaneous fluid concentrations and change rates, the Doerner–Hoskins equation is often integrated (e.g., Zhong and Mucci, 1995).

Table 3
Overview of monazite solubility studies at hydrothermal and magmatic conditions.

12. 13.	Cetiner et al. (2005)	Poitrasson et al. (2004)	Pourtier et al. (2010)	Tropper et al. (2011)	Ayers and Watson (1991)
Monazite	Synthetic	Synthetic	Synthetic	Synthetic	Natural
T (°C)	23 150	21 300	300 800	800	800 1100
P (GPa)	~3 10^{-6} ~5 10^{-4}	~3 10^{-6} ~9 10^{-3}	0.2 0.5	1	1 2.8
pH	0–2	2	1–8 (300 °C) 4–7.5 (650 °C)	4 (± neutral)	<2
NaCl (m)	0.01 0.91	–	0.2 2	0 55.6	1
Pressure effect	n.a.	n.a.	Weak	Weak	No
NaCl effect	No (weak at 150 °C)	n.a.	Pronounced	Pronounced LREE > HREE	No

The partitioning ratio depends on the reaction rate according to (Chernov, 1980):

$$K_D = K_D^0 + \left(K_{st} - K_D^0\right) e^{-\frac{D_S}{Rh}}$$

Where $K_D{}^0$ is the equilibrium partition ratio, K_{st} the partition ratio during the growth step, D_S the diffusion coefficient of the trace element in the crystal, R the linear growth rate and h the height of the growth step. The equation from Chernov (1980) takes into account the diffuse relaxation within a spherical crystal, but not in the fluid boundary layer. When crystal growth is fast or fluid replenishment is low, the supply of trace elements is often diffusion-controlled and trace elements are incorporated at the ratio of their diffusion coefficients in the fluid, which is normally close to unity (Fig. 7; Lakshtanov and Stipp, 2004; Möller et al., 1991; Wang and Xu, 2001). Experimental results from Zhong and Mucci (1995) indeed indicate rapid initial REEY uptake, followed by slower uptake. Nonetheless, partition ratios were found to be largely independent of precipitation rate, and this has been attributed to similar values of K_{st} and $K_D{}^0$ (Lakshtanov and Stipp, 2004). Finally, both experimental practice and natural systems illustrate that absolute REE concentrations in carbonates can be highly heterogeneous, with order of magnitude concentration variations on scales of 100 μm (Kontak and Jackson, 1995, 1999; Barker and Cox, 2011).

8.2. REEY partition ratios for calcite: no consensus, but highly compatible

Terakado and Masuda (1988) determined REE partition ratios with free drift experiments and reported apparent REE partition ratios between 2.5 and 10. Both the partition ratios and REE selectivity were dependent on the initial fluid's REE content. However, the application of free drift experiments to natural systems is limited because they allow for varying solution composition with variable and extremely fast growth rates, resulting in diffuse relaxation (Zhong and Mucci, 1995). Another problem with precipitation experiments is that the metastable calcite polymorph vaterite tends to precipitate and persist at low temperatures (Tsuno et al., 2002).

Controlled calcite precipitation from REE-rich artificial seawater resulted in much higher partition ratios between $>10^3$ and 10^2 with a systematic decrease from the LREE to the HREE (Zhong and Mucci, 1995). The calculated LREE partition ratios are on average an order of magnitude higher than the HREE ratios. LREE partition ratios exhibit a strong positive concentration dependency at concentrations between 1 and 10 ppm. This concentration dependency was attributed to increased competition for crystal sites at higher concentrations, with increasing preference for the better-fitting LREE. Finally, Tb, Dy and Gd showed anomalous partition ratios with respect to the neighboring REE in the lower part of the studied concentration range.

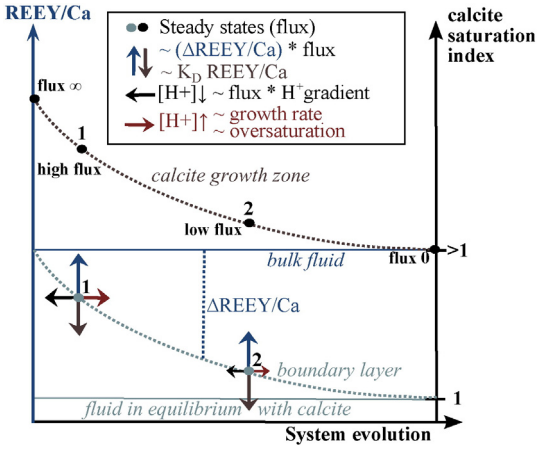

Fig. 7. Conceptual model showing steady state REEY/Ca ratios in calcite overgrowths precipitating from a oversaturated fluid at two different fluid fluxes, representing an advection- (1) and a diffusion-dominated system (2), respectively. In both cases, rapid initial calcite growth produces H^+, and decreases the REEY/Ca ratio of the boundary layer since the REEY are highly compatible. The decreasing calcite oversaturation then translates in a growth rate decrease (e.g., Reynolds, 1978). Eventually a steady state is established in function of the Δ [H^+] and Δ REEY/Ca gradients, their diffusivities and the fluid flux. Oscillation about the steady state due to metastable calcite growth could generate highly variable REEY concentrations that are experimentally observed.

Both Zhong and Mucci (1995) and Tanaka and Kawabe (2006) assume charge-balanced substitution with Na, based on a positive correlation between $\sum$REE and Na partition ratios. In the model from Zhong and Mucci (1995), competition between Ca^{2+} and $REECO_3^+$ is followed by competition of charge compensating $REECO_3^+$ or Na^+ ions for the adjacent sites. However, Na incorporation in calcite correlates with the number of crystal defects, and does not follow the Berthelot–Nernst distribution law (Busenberg and Plummer, 1985). Moreover, coupled substitution with Na^+ and OH^- is inconsistent with the observed proportionalities between aqueous Eu^{3+} and the cation mole fractions in calcite from both experimental and natural calcites (Curti et al., 2005; Lakshtanov and Stipp, 2004). For this reason, Lakshtanov and Stipp (2004) propose a solid solution between $Eu_2(x)(CO_3)_3$ and $CaCO_3$, as long as the incorporated Eu atoms are fewer in number than the intrinsic crystal defects. In the latter case, a different proportionality results, since Eu then controls the amount of defects.

Local charge balance would require the presence of vacant octahedral sites adjacent to Eu^{3+}, which is not supported by extended X-ray absorption fine structure (EXAFS) data (Elzinga et al., 2002). While satisfactory fits can be obtained for normal Ca-sites with 6-fold coordination (Withers et al., 2003), slightly longer bond lengths are found for Sm^{3+} and Nd^{3+}, although both ions are smaller than Ca^{2+}. The slight differences could be attributed to a 7-fold coordination in modified Ca-site, following bidentate REE-CO_3 bonding (Elzinga et al., 2002). Experimental data from Curti et al. (2005) provoked an alternative explanation, involving a mixture between two Eu species with 6-fold and 9-fold coordination respectively. Their results also suggest a crucial role of speciation during REE sequestration. The latter is also supported by data from natural calcites precipitated at low temperatures (Maskenskaya et al., 2015).

From the discussion above, it can be concluded that the currently available partition ratios are applicable in a limited range of conditions. In natural systems, similarities in REEY patterns between calcites and thermal waters (Göb et al., 2013) indicate that mineralogical control can be negligible in some cases. While the exact incorporation mechanism remains uncertain, all studies agree that the trivalent REEY are highly compatible in calcite, resulting in an enrichment with respect to the fluid.

8.3. Eu^{2+}–Eu^{3+} and Y–Ho fractionation by calcite

While the compatibility of divalent Eu in calcite has not been determined experimentally, its ionic radius of 117 pm is similar to strontium's radius of 118 pm, (Shannon, 1976). Because both ions are larger than Ca^{2+}, Bau (1991) predicted that divalent Eu would be rejected by the calcite mineral lattice. Distribution ratios for Sr between calcite and hydrothermal fluids have been determined experimentally and increase from 0.04 to 0.06 between 40 and 200 °C (Malone and Baker, 1999). Interestingly, theoretical predictions based on linear regression of Gibbs free energies and ionic radii predict that Sr^{2+} compatibility is one order of magnitude higher than observed, albeit still incompatible (Wang and Xu, 2001). Nonetheless, if Sr^{2+} is a good geochemical analog for divalent Eu, the partition ratio of divalent Eu is likely much lower than those of the highly compatible trivalent REEY.

Controlled precipitation experiments from Tanaka and Kawabe (2006) indicate that the partition ratio of Y is about 0.6 times the partition ratio of its geochemical twin Ho. This Y–Ho fractionation was also predicted based on EXAFS results by Tanaka et al. (2008), and underlines the important role of covalent bonding aspects (Jordan et al., 2011).

8.4. Mineralogical control by other carbonate minerals

While partitioning data for dolomite is lacking, high compatibilities are expected since dolomite is composed of alternating calcite ($CaCO_3$) and magnesite ($MgCO_3$) layers. In natural systems, limited differences in pattern shapes between hydrothermal calcites and dolomites (e.g., Hecht et al., 1999; Roberts et al., 2009) suggest that fractionation between these phases is relatively unimportant. In carbonatites, calcite was found to contain about 5 times more REEY than associated dolomite crystals, with limited REEY fractionation (Dawson and Hinton, 2003).

Magnesite is thought to reject $LREE^{3+}$ (radius ~100 pm) while more easily accepting $HREE^{3+}$ (radius ~90 pm) because the Mg^{2+} radius (72 pm) in 6-fold coordination is more similar to the latter (Bau and Möller, 1992; Shannon, 1976). For the same reason, LREE are expected to be less easily accepted than HREE in the ankerite structure ($CaFe(CO_3)_2$), which commonly occurs as a solid solution with dolomite. A similar reasoning could be made for carbonates with Fe (67 pm) and Mn (61 pm) such as siderite ($FeCO_3$) and rodochrosite ($MnCO_3$) (Bau and Möller, 1992; Shannon, 1976). However, in light of the EXAFS evidence for the modification of Ca sites by REEY (Curti et al., 2005; Elzinga et al., 2002), mineralogical control by other carbonate phases requires confirmation by experimental studies.

9. Coprecipitation

9.1. Apatite

The REEY concentrations in natural apatites are generally significantly higher than those in associated dolomites, e.g., by a factor ~100 (Banner et al., 1988). Calcite and apatite coprecipitating from carbonatitic magmas give much lower apparent apatite/calcite partition ratios, declining from about 4 for the LREE to about 2.5 for the HREE (Dawson and Hinton, 2003). Unlike calcite, apatite contains two different Ca sites with radii of 106 and 118 pm respectively (Hughes et al., 1989). This has important implications for Eu^{2+} incorporation, as the radius of the larger site and Eu^{2+} is near-identical, resulting in high partition ratios for divalent europium in apatite.

9.2. Monazite-Ce and allanite-Ce

Both monazite-Ce and allanite-Ce contain REE as major elements in their crystal lattice and are strongly LREE-selective in magmatic systems (Mahood and Hildreth, 1983; Yurimoto et al., 1990). Because of this, these minerals are thus expected to significantly lower the availability of LREE during coprecipitation. Igneous allanite-Ce can be depleted in LREE during equilibration with fluor-rich hydrothermal fluids (Wood and Ricketts, 2000). In this case, close association with secondary precipitates such as fluorite, thorianite and a REE-phosphate indicates limited mobilization (μm-scale), owing to the low solubility of the alteration products. Nonetheless, there are indications that REEY contained in allanite-Ce can be remobilized over much larger distances (tens of meters) by hydrothermal fluids around volcanogenic massive sulfide deposits (Genna et al., 2014). Because both monazite-Ce and allanite-Ce contain REEY as major elements and are strongly LREE selective, coprecipitation with these minerals strongly influences the REEY availability for hydrothermal carbonate minerals. Post-depositional modifications.

The preservation of the primary REEY signature in hydrothermal carbonates is a prerequisite to deduce the REEY budget and the physicochemical properties of their parental fluid. However, secondary processes such as recrystallization and alteration by post-depositional fluids can disturb the pristine trace element and isotopic composition of hydrothermal carbonates. Carbonates deposited in shallow marine and continental environments are susceptible to REEY signature modification by meteoric and diagenetic fluids (e.g., Zhao and Zheng, 2013). Recrystallization during dolomitization only seems to affect carbonate REEY distribution on a small scale (Banner et al., 1988; Hecht et al., 1999). Nonetheless, super-imposed concentration variations in the redox-sensitive REE, in combination with a general increase of $\sum$REE, have been successfully used to proxy influx of post-depositional fluids of contrasting Eh–pH conditions compared to the initial hydrothermal fluids (Spangenberg and Fontbote, 1995).

Calculations from Banner et al. (1988) suggested that extremely high water/rock ratios ($>10^5$) are needed to alter carbonate REEY signatures by diagenetic fluids, while for Sr this can be as low as 30. Nd–Sr data on hydrothermal veins confirm that Sr is indeed more easily reset than Nd (Barker et al., 2009; Van Wilderode et al., 2015). However, the diagenetic fluid from Banner et al. (1988) contained ~200 times less Nd than seawater, with a Nd/Ca ratio ~700 that is times lower (Bau et al., 1997; Turekian, 1968). Therefore, most hydrothermal brines require significantly lower fluid rock ratios to alter the Nd signature. This might account for the variable resetting of Nd in the study from Barker et al. (2009). Nonetheless, successful Sm–Nd dating on carbonates demonstrates that Nd is not always reset in hydrothermal systems (Henjes-Kunst et al., 2014; Oberthür et al., 2009).

Depending on the saturation of calcite and REEY in the interacting fluid, interaction follows different scenarios. Interaction with calcite-supersaturated fluids essentially leads to calcite overgrowths (Section 9). Therefore, we will focus here on interaction with calcite-undersaturated fluids. In this case, the most mobile REEY are expected to be preferentially removed by the fluid, generally in the order: $Eu^{2+} >> LREE^{3+} >$ or $< HREE^{3+} >> Ce^{4+}$. Furthermore, Y^{3+} is more mobile than Ho^{3+} in the presence of F^- or Fe–Mn oxyhydroxides (Bau et al., 1996; Bau and Dulski, 1996, 1999). The relative mobility of LREE versus HREE depends on their speciation in the fluid. For instance, in fluids where Cl^- or F^- complexes dominate REEY speciation, transport capacities for the LREE are higher than for HREE (Migdisov et al., 2009), and vice versa for fluids dominated by CO_3^{2+} or OH^- complexes (Haas et al., 1995). Since calcite dissolution increases the pH of the fluid and releases CO_3^{2-} (Eqs. (5), (6)), this favors preferential HREE removal by the fluid. The REEY loss or gain is hard to predict, as it depends on whether the Ca/REEY ratio removed by the undersaturated fluid is higher or lower than in the unaltered precipitate, respectively.

Ultimately, the REEY signature change during post-depositional interaction depends on the mineral stability during remobilization, the transport capacities of the interacting fluid, its saturation state for each individual REEY, and the degree of equilibration during interaction. Detailed petrographic studies are essential, as they provide clues for multiple growth events or recrystallization. For instance, a change in cathodoluminescence color can indicate variations in redox-sensitive

elements such as Fe and Mn, or REEY, since the lanthanoids also activate luminescence.

In practice, the effects of post-depositional processes can be estimated by systematically comparing carbonate signatures with different degrees of inferred post-depositional modification. In the presence of F^- or Fe–Mn oxy-hydroxides, these effects could be monitored by variations in Y/Ho ratios. For highly oxidizing supergene fluids, REEY loss or gain can be monitored by increase or decrease of the Ce/Ce^*_N ratio, respectively.

10. Summary and application of the source–sink system

In this section, several flow charts are provided that summarize the hydrothermal geochemistry of the REEY discussed in previous sections (Figs. 8–10), before several examples are discussed which illustrate REEY interpretation in specific cases. While the diagrams cover the main processes that govern REEY pattern evolution from source to sink, the diagrams are by no means intended to be exhaustive. Furthermore, the specifics of the studied hydrothermal systems may demand a modification of the approach. Nonetheless, the general concepts portrayed by these diagrams can facilitate interpretation of REEY patterns. While the complex interaction between processes commonly precludes identification of the role of individual processes (Figs. 8–10), the resulting pattern characteristics give an indication of the dominant processes.

The flow charts are designed to back-track the REEY composition towards the source-inherited characteristics, starting with the composition of the precipitated carbonate minerals. Firstly, the REEY fractionation between the measured REEY composition and the 'parental fluid' composition is considered. We define the parental fluid as the entire fluid volume from which the analyzed crystals and coprecipitating phases originated. This parental fluid thus contains all REEY atoms that were distributed between the complexes that were retained in the fluid, the analyzed carbonate minerals and the coprecipitating

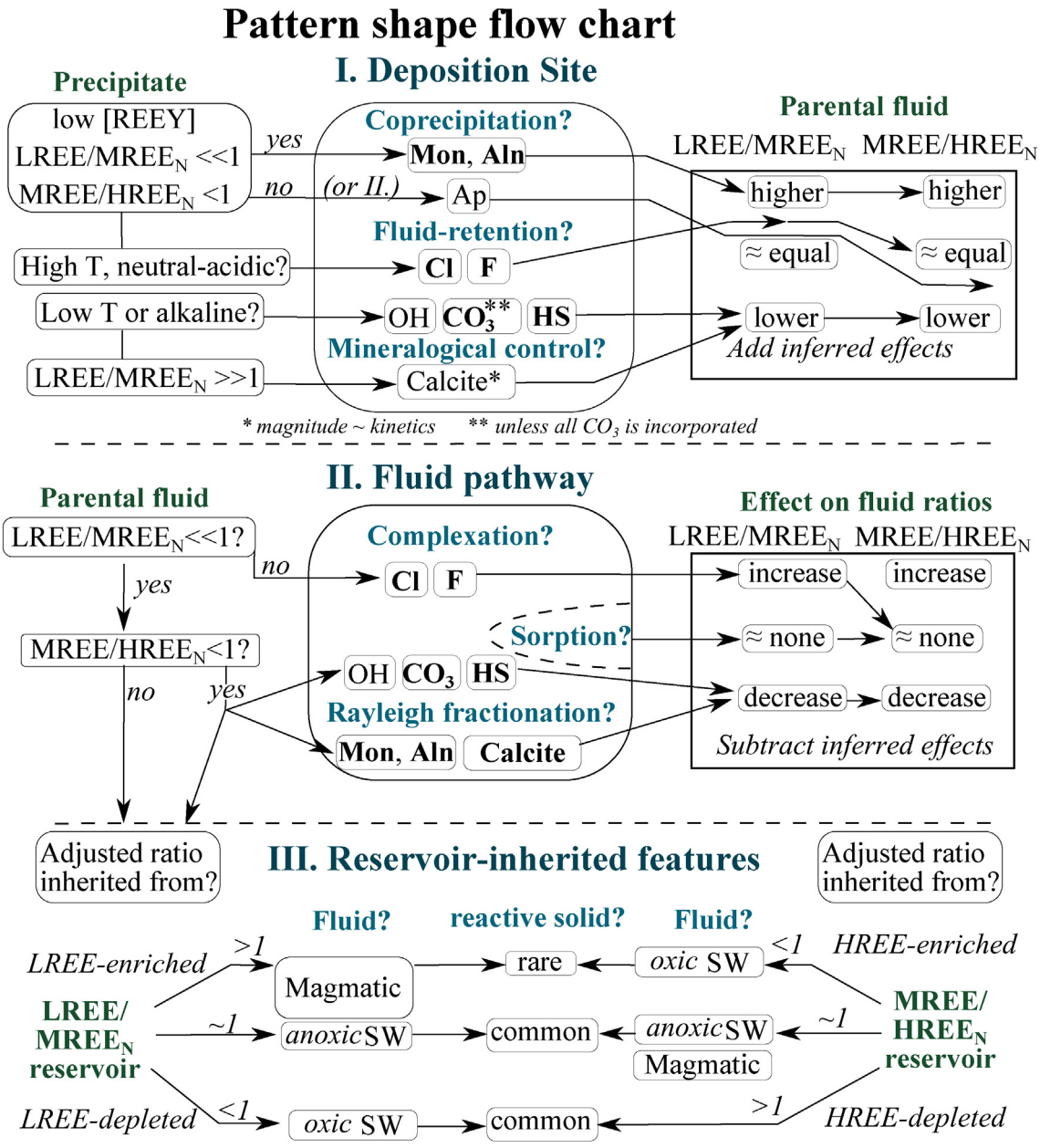

Fig. 8. Flow chart illustrating the main processes influencing the REEY pattern shape along the fluid pathway. Pattern shape characteristics with respect to upper crust reference compositions such as UCC and PAAS. Abbreviations: humic substances (HS),apatite, (Ap), allanite (Aln), monazite (Mon), seawater (SW), light, mid and heavy rare earth elements (LREE, MREE and HREE respectively). See text for references.

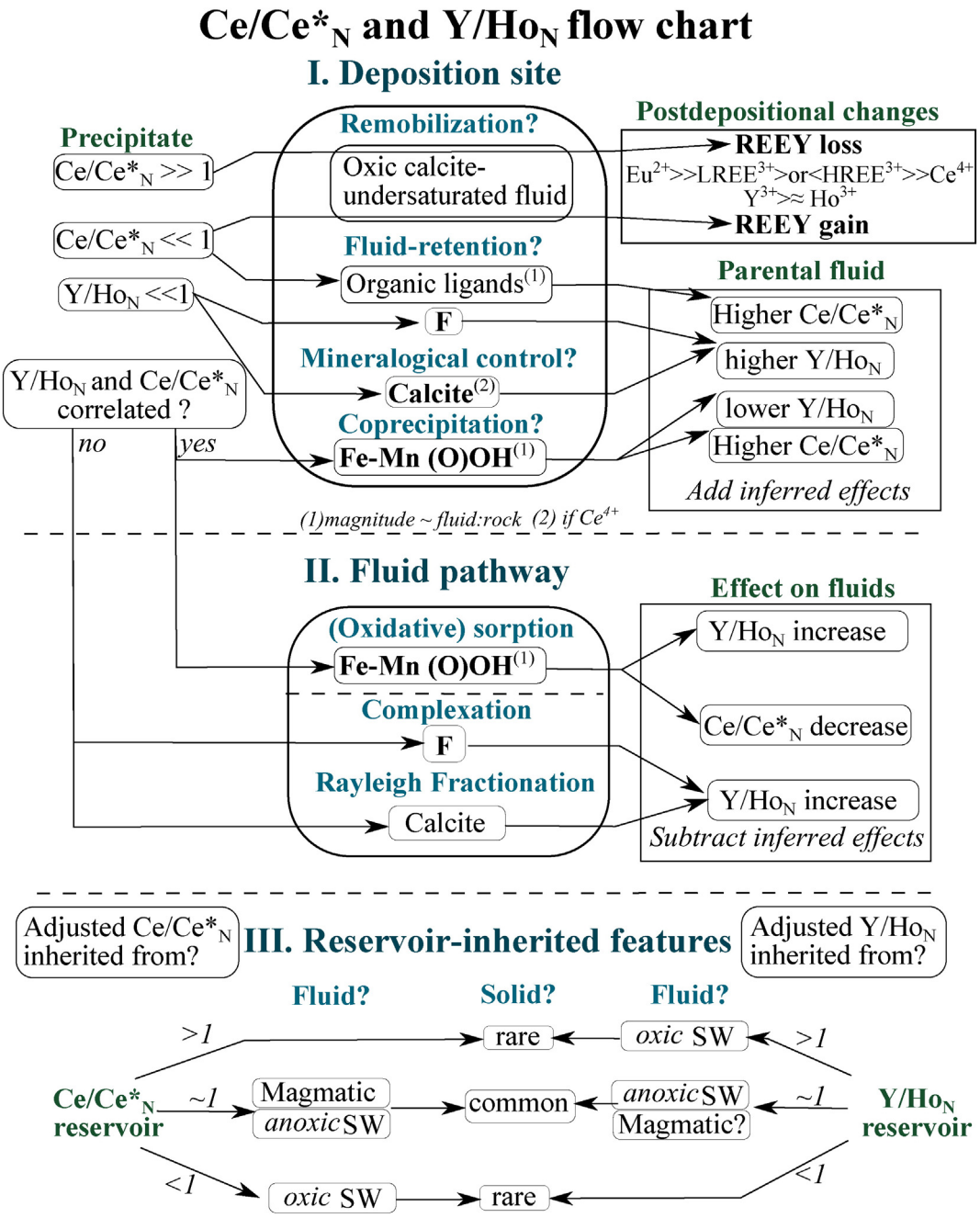

Fig. 9. Flow chart illustrating the main processes influencing Ce/Ce^*_N and Y/Ho_N along the fluid pathway. Relative mobility during remobilization tends to decrease from divalent to tetravalent ions, relative LREE–HREE mobility depends on fluid speciation, where Cl^- and F^- facilitate LREE transport and CO_3^{2-} and, to a lesser degree, OH- facilitate HREE transport. Y^{3+} is more mobile than Ho^{3+} in the presence of F^- or Fe–Mn oxides. Valid for crustal and chondrite-based reference compositions. Abbreviations: seawater (SW). See text for references.

phases. In the second part, the effects of the REEY fractionating processes operating along the fluid pathway are estimated. Once these effects are stripped from the parental fluid composition, the corrected patterns can be compared with the source composition. The flow charts thus consist of three main parts:

I. At the deposit site, the effects of mineralogical control, coprecipitation, fluid retention and sometimes post-depositional remobilization are assessed to recalculate the parental fluid composition. Potential coprecipitating phases are readily apparent from petrographical information, while temperature constraints and constraints on the fluid composition give an indication of the main complexes, and the expected redox state of Eu.
II. Starting from the estimated parental fluid composition, the main processes along the fluid pathway from source to deposit site can be estimated, taking into account the range of possible inherited characteristics, and the inferred main complexes. Where the fluid pathway is not exposed, Rayleigh fractionation can only be deduced from its effect on the pattern characteristics of the parental fluid versus the range of possible inherited values.
III. In the lower part, a range of possible inherited source characteristics is given in terms of pattern shape ratios, Eu/Eu^*_N, Ce/Ce^*_N and Y/Ho values. Usually, it is not possible to trace the values back to the sources, with the exception of Eu anomalies in low temperature fluids, and sometimes Y/Ho values. However, as discussed in Sections 3 and 4, the range of potential inherited values is quite limited for many REEY characteristics.

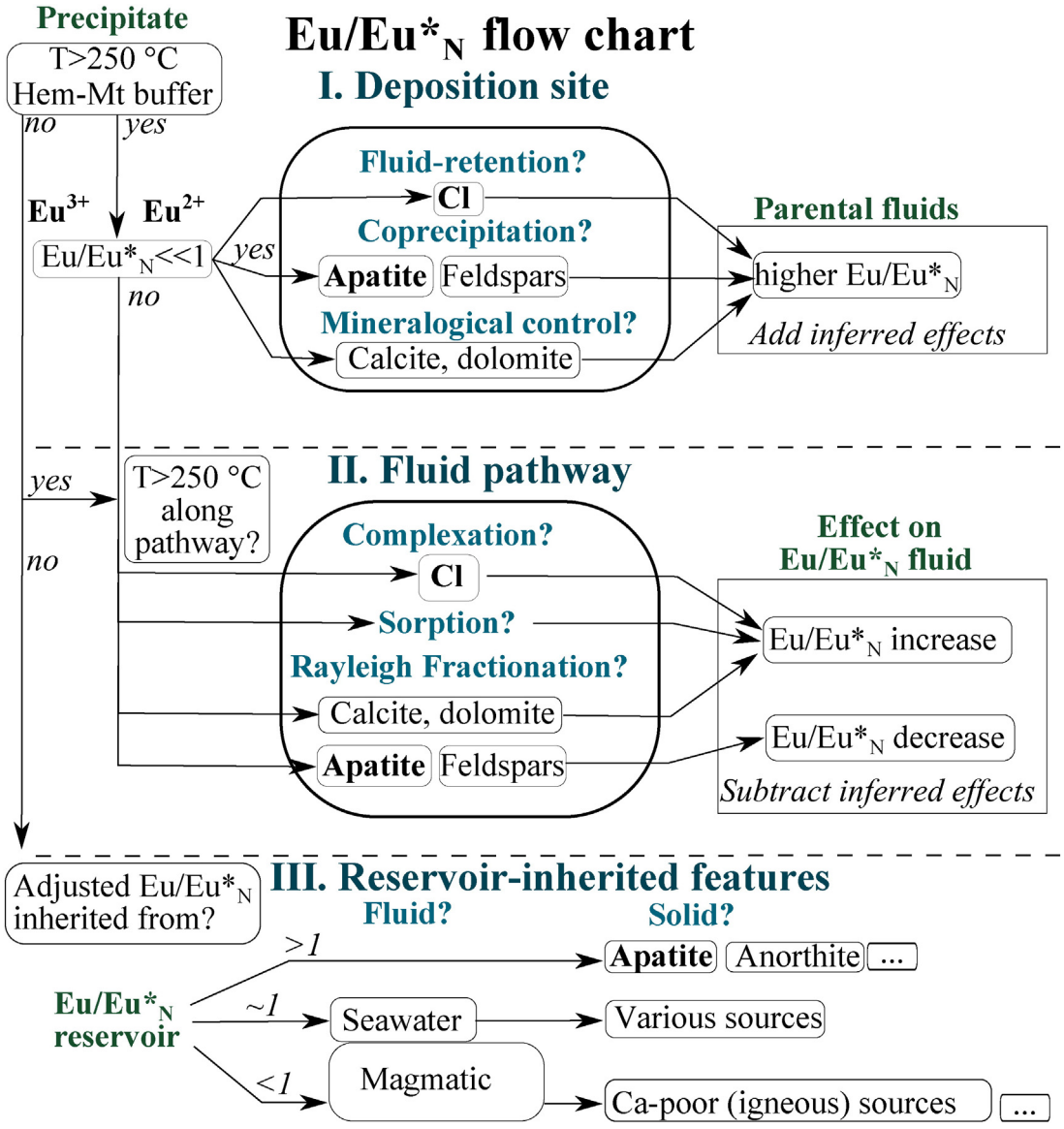

Fig. 10. Flow chart illustrating the main processes influencing Eu/Eu_N^* along the fluid pathway. Valid for patterns normalized over the UCC, PM and chondrite compositions. When normalized over PAAS, values below unity can reflect a reference choice artifact, depending on the source composition. Abbreviations: hematite (Hem), magnetite (Mt). See text for references.

The application of these schemes is illustrated for a number of examples covering formation temperatures from near ambient calcite coatings to temperatures associated with greenschist metamorphism (~400–450 °C). The main relevant characteristics for each example are presented in Table 4, along with representative REEY ratios for each pattern type within a study area. PAAS is chosen as the reference composition for all examples to maintain consistency and because this is the most widely used for normalization, although it is not necessarily the most suitable reference composition.

10.1. A fictional example

As an introduction to the backtracking process, the following example is shown in Table 4 and Fig. 11. This fictional calcite coprecipitated with monazite in fractures at the border of a granite pluton, and Mn-hydroxides are rimming some of the fractures along the pathway. Fluid inclusion evidence in the form of the salinity-salt composition and crush leach data indicates that mineralization occurred at temperatures around 180 °C from a seawater-like fluid that interacted with the granite pluton.

The calcite has a strong LREE depletion (La/Sm_N 0.02) and moderate MREE–HREE fractionation (Dy/Yb_N 0.50), at relatively low concentration levels ($\sum$REE 15 ppm). The pattern shape flow chart (Fig. 8) indicates that $LREE/MREE_N$ and $MREE/HREE_N$ ratios in the parental fluid were likely higher, considering the preferential LREE (and MREE) uptake by monazite. Nonetheless, mineralogical control by calcite would still result in higher ratios compared to the remaining fluid, depending on the open or closed nature of the system. Coprecipitation with monazite would also account for the relatively low $\sum$REE of 10 ppm in calcite, although this also depends on the open or closed nature of the system, and the REEY/Ca ratio in the parental fluid.

Along the short fluid pathway, Cl and F are likely transport agents, and these complexes form more stable complexes with the LREE, reducing the activity of the free or weakly bound REE ions, and thus increasing the transport capacity of the fluid, mainly for the LREE. Therefore, the source-inherited $LREE/MREE_N$ ratio could be somewhat lower than in the parental fluid.

The high Y/Ho ratio (30) despite the mineralogical preference for Ho by calcite (Fig. 9) could reflect preferential REE uptake by sorption to Mn-hydroxides observed along the pathway, which would also

Table 4
Summary of deposit characteristics for the examples discussed in Section 11, along with representative REEY ratios for the discussed calcite and dolomite phases. Typical values and ranges for a number of fluids and reservoirs are also given for comparison. Abbreviations: ankerite (ank), calcite (cal), dolomite (dol), equigranular (eqg), acicular (acic), humic substances (HS).

Example	Type	T (°C)	Potential coprecipitation (all stages)	Source fluid	Potential solid sources	Expected main complexes	Stage	Pattern/PAAS							∑REE (ppm)
								LREE/MREE La/Sm_N	LREE/HREE La/Yb_N	MREE/HREE Dy/Yb_N	Ce/Ce^*_N	Pr/Pr^*_N	Eu/Eu^*_N	Y/Ho mass	
Fictional	Introductory example	180	Monazite	Seawater	Granite	Cl, F	cal	0.02	0.01	0.5	0.50	1.16	0.8	30	10
Laxemar[1]	Fracture coatings in crystalline rocks	≤50	Phyllosilicates, Mn oxyhydroxide, goethite, pyrite	Seawater, meteoric water	Granites, quartz–monzonites, gabbros	CO_3 HS	Eqg. Acic.	14 3.5	156 6.8	2.0 1.4	0.64 0.76	0.84 0.85	1.0–1.4 0.7–1.8	n.a.	340 440
Dikulushi[2]	Vein-type base metal mineralization in dolomite-shale host	100–200 ~65	Quartz, sulfides	Basinal brine, meteoric water	Shale, siltstones, dolomites	Cl F?	cal 1 cal 3 dol 3	0.14 0.12 0.02	0.25 0.17 0.03	1.8 1.4 1.6	0.92 0.90 0.70	1.01 1.01 0.83	0.5–1.8 0.7–1.5 0.4	22.9 23.8 23.9	350 58 140
Bracemac–McLeod[3]	Volcanogenic Massive Sulfide	250 300	Apatite, allanite, quartz, sulfides	Archean seawater, magmatic fluid?	Rhyolites, gabbros, andesitic tuff	Cl F	ank cal 1 cal 2 apat	0.09 0.15 0.46 0.28	0.10 0.14 2.13 1.51	1.7 1.4 3.4 3.9	1.02 0.87 0.89 0.99	0.87 0.92 0.97 0.92	5.0 2.8 1.3 4.6	27.8 29.2 26.7 24.8	32 52 311 2160
Nkana[4]	Siltstone-hosted Co ± Cu deposit	≤200–450	Apatite, quartz, sulfides, anhydrite	Basinal brine	Granites, gneisses, metagabbros, carbonaceous siltstones	Cl F?	Type I Type II Type III Type IV Type X	0.28 0.20 0.20 0.20 0.27	0.58 0.11 0.03 0.08 0.22	1.8 1.1 0.6 1.0 1.0	0.94 0.94 0.93 0.91 0.94	1.08 0.94 0.86 0.99 0.99	2.8 1.3 0.8 2.2 0.6	22.3 23.0 25.3 25.1 33.0	44 32 64 25 150
Seawater (oxic)		Bau et al. (1997)						0.12	0.15	0.63	0.32	1.22	1.2	46	3E-5
Seawater (anoxic)								0.48	0.57	0.88	1.83	0.61	0.9	36	9E-5
Silicate leachates		Möller et al. (1997b)					min	0.08	1.02	0.11	0.88	0.96	0.2	–	0.03
							max	0.59	3.07	0.63	1.06	1.06	4.4		0.33
Magmatic fluids		Banks et al. (1994)					min	1.32	1.51	0.89	0.85	0.84	1.0	–	193
							max	3.25	4.54	1.87	1.00	1.07	2.9		1290

[1]Maskenskaya et al. (2015), [2]Haest et al. (2009, 2010), [3]Genna et al. (2014) [4], Brems et al. (2009), Muchez et al. (2010). [(2), (4)] REEY data from Debruyne et al. (2013), cf. supplementary table A.

preferentially incorporate Ce, implying that Ce/Ce^*_N value inherited from the source is higher than 0.50 (Fig. 9). Even so, the adjusted Ce/Ce^*_N ratio of the calcite (>0.50) is still more easily reconciled with inheritance from an oxidizing seawater fluid, rather than a magmatic fluid of pure granitic origin.

Low mineralization temperatures imply that Eu was trivalent in the fluid. Under these conditions, it is not significantly fractionated from the neighboring REE during fluid transport and calcite precipitation. Consequently, the observed negative Eu anomaly (Eu/Eu^*_N 0.8) is then directly inherited from the sources (Fig. 10), in this case a marine fluid and the reactive granite composition.

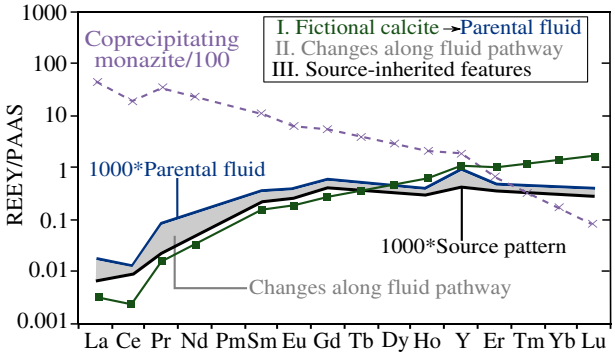

Fig. 11. Backtracking of a REEY pattern illustrated for a fictional calcite precipitate discussed in Subsection 11.1. The REEY of the parental fluid are contained in the residual fluid, the calcite and in coprecipitating monazite. Subtracting the changes along the fluid pathwaydue to sorption, complexation and precipitation of supersaturated phases finally gives the source-inherited characteristics.

10.2. Calcite coatings in Laxemar, Sweden (≤50 °C)

In Laxemar, calcite coatings are present on fracture walls in crystalline rocks (Table 4; Fig. 12A; Maskenskaya et al., 2015). The calcites likely precipitated in equilibrium with low-temperature fluids (≤50 °C) within the last 10 million years. Earlier fracture phases precipitated at higher temperatures and are mineralogically complex and contain epidote, phyllosilicates, Fe–Mn oxyhydroxides and REE carbonates as the main REE carriers. The parental fluids for the most recent precipitates are seawater and meteoric water, percolating into the granitic, quartz monzonitic and gabbroitic host rocks (Table 4; Mathurin et al., 2014). The major and trace element composition of the present-day groundwater is also available, including the REEY (Mathurin et al., 2014). Since the latter is likely a good proxy for paleo-groundwater compositions, it provides an excellent starting point for a source–sink approach. Currently, fluids in Laxemar show fairly flat REEY patterns when normalized over PAAS, with slight LREE depletions in fracture water and small LREE enrichment in regolith waters (Mathurin et al., 2014). Speciation calculations indicate that LREE are dominantly contained in humic substances (~70%), carbonates (~20%) and minor aqueous, chloride and sulfide complexes (~10%), whereas HREE are almost exclusively contained in humic substances (>90%) and minor carbonates (<10%). The latter indicates that humic substances are strongly HREE selective (Fig. 8).

The calcite coatings contain highly variable REE concentrations with ∑REE differences over three orders of magnitude. Their total REE content can be extremely high, up to 2300 ppm ∑REE, despite

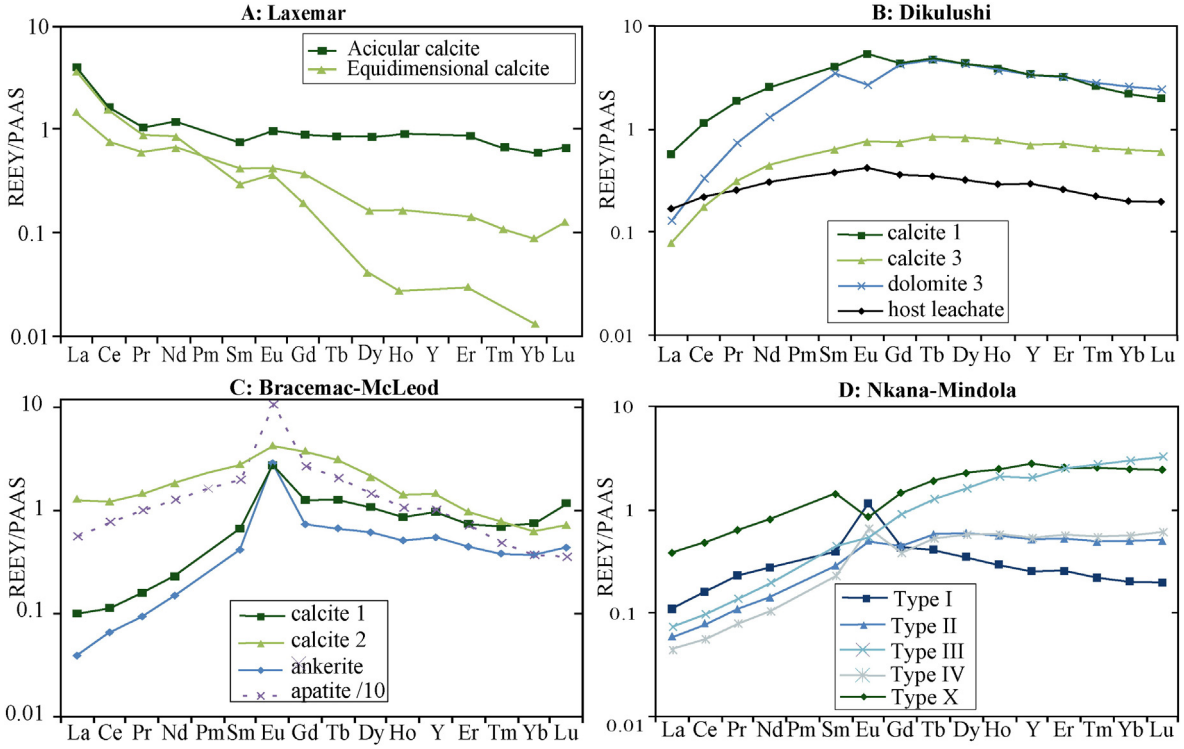

Fig. 12. Representative REEY signatures for hydrothermal carbonates from the Laxemar, Dikulushi, Bracemac–McLeod and Nkana–Mindola deposits. Patterns normalized over the PAAS composition.

precipitating from fluids with low REE transport capacities. Mg-rich acicular calcites are restricted to the upper 260 m and generally show less REE fractionation. Most coatings show pronounced LREE-enriched patterns when normalized over PAAS (Fig. 12A), and this is most pronounced in a subset of the blocky calcites, both at shallow depths (<260 m) and deeper in the succession. The high concentrations can be linked to Ca-poor fluids and limited REE/Ca decrease in the fluids during precipitation of the small coatings. The LREE enrichment can partly be explained by precipitation from fluids wherein Ca availability limits the calcite precipitation (Fig. 8; Bau and Möller, 1992). The HREE are then retained in stable humic substances and CO_3^{2-} complexes, which are the dominant REE transporting species at the inferred mineralization conditions (Mathurin et al., 2014). The LREE-selectivity of calcite would then further amplify this trend (Fig. 8), as long as crystallization occurs in an open system that allows maintaining high REE/Ca ratios in the fluid during precipitation. Under such conditions, a positive relation is expected between La/Lu_N ratio of the coatings and their total REE concentrations. Conversely a negative correlation between $\sum$REE and the incompatible element Sr is expected. Neither is observed, indicating that mineralogical control alone cannot account for the LREE-enrichment. Therefore, it seems that complexation-driven fractionation by carbonate species and humic substances is the dominant process causing the LREE enrichment in the precipitates. The flatter patterns in the acicular coatings are likely related to precipitation from more HREE-enriched marine waters, likely containing less humic substances. While this is supported by their high Mg-content, these coatings did not inherit a negative Ce anomaly characteristic for seawater-derived fluids (Fig. 9). Average Pr/Pr^*_N values around 0.85 (Table 4) indicate a positive La anomaly, rather than a negative Ce anomaly (Fig. 12A). This feature is likely inherited from the parental fluids, where it likely results from different speciation for La compared to the other REE, with less stable complexes resulting in increased availability during crystallization.

At near-ambient precipitation temperatures, Eu is exclusively trivalent, and the Eu anomalies are directly inherited from the source fluids and the solid source area (Fig. 10). The measured Eu/Eu^*_N values are variable (Table 4), and on average slightly above unity, as would be expected by direct inheritance from marine fluids compared to PAAS (marine $Eu/Eu^*_N \sim 1.2$). Slightly lower Eu/Eu^*_N values (~0.7–1.0) and occasionally higher values of ~1.5–2 likely reflect REE addition by granitic or gabbroitic basement rocks respectively (Fig. 10).

Data from current groundwater compositions allowed Maskenskaya et al. (2015) to back-calculate the paleo-groundwater compositions. On average, calculated La/Yb_N ratios were similar to current values, yet extended one order of magnitude below and above the current range. Maskenskaya et al. (2015) point out that discrepancies can result from the colloidal REE fraction, included in the groundwater analyses (Mathurin et al., 2014), yet most likely unavailable for incorporation in calcite. Additionally, the concentration-dependent partition ratios from Zhong and Mucci (1995) at REE concentrations of 11 ppm are likely inappropriate for the studied groundwater concentrations. Nonetheless, average back-calculated La/Yb_N ratios are remarkably similar to current groundwater compositions. Moreover, back-calculated La/Ca and Yb/Ca ratios appear strongly influenced by carbonate speciation, confirming the crucial role of carbonate complexes during REE sequestration at low temperatures.

10.3. Base metal mineralization at Dikulushi, DR Congo (<100–200 °C)

The Congolese Dikulushi deposit is characterized by a two-phase base metal – Cu–Ag sulfide mineralization hosted by Neoproterozoic sedimentary rocks, with quartz and calcite or dolomite as the main gangue minerals. This deposit was intensely studied using petrography, fluid inclusions, Cu and Pb isotopes, making it a suitable test case for a REEY-based study. Fluid inclusion data indicates that the Cu–Pb–Zn–Fe mineralization at Dikulushi originated from a high saline–medium temperature H_2O–$CaCl_2$–NaCl fluid (20–25 wt.% NaCl eq.; 100–200 °C; Haest et al., 2009). A second Cu–Ag mineralization is interpreted as a remobilization of the first phase, whereby mineralization results from mixing of a moderately saline fluid (>19 wt.% NaCl eq.) with a

low salinity fluid (3 wt.% NaCl eq.) in approximate thermal equilibrium with their host rocks at ~65 °C (Haest et al., 2009). The mineralizing fluids are thus most likely derived from evaporated seawater or re-dissolution of crustal evaporites, which consecutively interacted with the Katanga basin sediments, mafic intrusions into these sediments, and potentially the underlying Proterozoic basement (e.g.., Van Wilderode et al., 2015). Lead isotope ratios are heterogeneous and indicate distinct solid source areas with incomplete mixing between the endmember compositions (Haest et al., 2010). Finally, Cu isotope ratios vary with the depth from the surface and the distance to the center of the deposit, indicating supergene remobilization (Haest et al., 2009).

Mineralization temperatures below 200 °C imply that Eu was trivalent during hydrothermal transport. This considerably simplifies interpretation of the Eu anomalies, since Eu is then mostly trivalent and not significantly fractionated from the neighboring REE (Fig. 10). Consequently, the observed anomalies are directly inherited from their sources. Variable Eu/Eu^*_N ratios between 0.5 and 1.8 in the calcites (Table 4) thus indicate equilibration with different source areas, in accordance with the large heterogeneity in observed Pb-isotope compositions (Haest et al., 2010).

Calcite and dolomite Pr/Pr* ratios around unity in combination with Ce/Ce^*_N values of 0.7–0.9 indicate positive La anomalies (Table 4; Bau and Dulski, 1996). This suggests a limited role for Fe–Mn oxyhydroxides and indicates that Ce was trivalent during mobilization. The measured Y/Ho mass ratios of 22–23 are around 0.9 times the PAAS ratio. Partition ratios from Tanaka and Kawabe (2006) indicate that calcite prefers Ho over Y by a factor of ~1.66. Assuming that the carbonates crystallized in an open system with continuous replenishment, this corresponds to Y/Ho ratios up to 1.6 times the PAAS-value, constraining a maximum estimate for the parental fluid ratio. While the real value is likely lower, values above unity can be realistically assumed. Such values indicate F-complexation driven Y-enrichment or preferential HREE-sorption to Fe–Mn oxides (Fig. 9). However, the lack of negative Ce anomalies is inconsistent with sorption to Fe–Mn phases. Moreover, the Y/Ho and Ce/Ce* ratios are not correlated. Post-depositional lanthanoid enrichment in oxidizing conditions would also lead to negative Ce anomalies, and possibly modify Y–Ho ratios, depending on the mobilization conditions (Fig. 8).

The $\sum$REE-values in the calcite and dolomite precipitates associated with the Cu–Pb Zn mineralization vary between 94 and 757 ppm. The calcite associated with the Cu–Ag mineralization contains less REE ($\sum$REE ~60 ppm, Table 4). The observed concentrations are relatively elevated for hydrothermal carbonates, indicating parental fluids with high REE/Ca ratios, especially in the calcites associated with the base metal mineralization. Partition ratios similar to those in seawater would translate to average REE/Ca ratios around 10–80 times higher than seawater, even though the expected Ca-content in crustal fluids is much higher, likely at the percentage-level (Table 1). Such high concentrations favor crystallization in an open system, as closed systems would experience a rapid decline in fluid REE/Ca ratios due to rapid preferential REE uptake by calcite.

Calcite and dolomite REEY patterns associated with the base metal and Cu–Ag mineralization are sub-parallel (Fig. 12B), with upwards convex to square-root shapes when normalized over the Upper Continental Crust composition (Debruyne et al., 2013). The carbonates display a strong LREE depletion (La/Sm_N ~0.06), generally associated with a HREE depletion (Dy/Yb_N ~1.6; Table 4). The LREE depletion is more pronounced for the dolomites than for the calcites, which could reflect mineralogical control. The upwards convex pattern observed can be inherited from the primary fluids and crustal sources, subsequently modified Rayleigh fractionation of REEY-bearing minerals, sorption and complexation-induced REEY fractionation along the fluid pathway. At the deposition site, REEY can also be fractionated by retention in fluid complexes and incorporation in coprecipitating minerals (Fig. 8), in this case mainly galenite, sphalerite and quartz. The upwards convex shapes (Fig. 12B) are reminiscent of easily leachable REEY content in silicate sources, albeit with a more pronounced LREE depletion. The pronounced LREE depletion is a fairly common characteristic of hydrothermal carbonates (Bau and Möller, 1992; Wagner et al., 2010). Unless the reactive source composition is extremely LREE-depleted, this suggests that LREE depletion by LREE-retention in stable complexes at the deposition site or by Rayleigh fractionation of LREE-selective minerals (e.g., calcite, monazite) along the pathway are dominant processes (Fig. 8). Rayleigh fractionation alone would result in a relative HREE-enrichment, whereas flat to depleted HREE patterns are more common in Dikulushi (Fig. 12B). The HREE depletion could be a source characteristic, as the smaller HREE are retained in stable minerals (e.g., zircon; cf. Lüders et al. (1993)). HREE are generally more compatible than LREE and thus preferably retained in the solids (cf. Shibata et al. (2006)).

10.4. Volcanogenic massive sulfide deposits: Bracemac–McLeod (250–300 °C)

Volcanogenic massive sulfide (VMS) deposits provide a unique opportunity to study REEY mass transfer along the entire pathway, since these deposits are closely associated with their sources. The example below is based on an exemplary REEY study from Genna et al. (2014), translated to a process-centered approach, while highlighting a few additional aspects. The 2.7 Ga old Bracemac and McLeod deposits in the Matagami mining camp (Canada) are hosted by an andesitic tuff. The host tuff is underlain by a thick rhyolitic volcanite, crosscut by several gabbroitic dykes in the vicinity of the deposits. A large sericitization zone (~250 °C) surrounds the mineralization and is overprinted by a chloritization (~300 °C) associated with a Zn–Cu–Ag mineralization. The alteration zones around this VMS deposit is characterized by REEY remobilization, with varying LREE enrichments and depletions on scales of tens to hundreds of meters (Genna et al., 2014). The mineralizing fluids were likely modified Archean seawater (Genna et al., 2014). The main solid source area during water–rock interaction for this subseafloor replacement mineralization is most likely the Watson Lake Rhyolite, in combination with gabbroitic dykes, the Bracemac Rhyolite and the unaltered tuffite. While the glassy matrix of the source area is currently completely replaced by secondary minerals, it was possibly still present during mineralization, and all REEY contained in glass phases are expected to be released congruently (Möller and Giese, 1997).

Genna et al. (2014) combined whole rock REEY analyses of altered and unaltered andesitic host rock with LA-ICP-MS analyses of hydrothermal disseminated and vein calcite, rare ankerite associated with sulfide ores, finely disseminated fluor – (hydroxy-) apatite in the chloritized zone and primary or hydrothermal allanite. The unaltered host tuff outside the mineralized zone is used as a reference composition for REEY depletion and alteration around the deposits. Interestingly, this deposit was generated prior to significant oxygenation of the atmosphere (Holland, 2006), thus Ce was likely exclusively trivalent and hence not fractionated from the other REE during mineralization. Hence, any deviations likely reflect superimposed processes that occurred much later. Average Ce/Ce^*_N values between 0.87 and 1.02 (Table 4) indeed closely correspond to the current host and source rock ratios (0.91–1.04), confirming that they are directly inherited.

Y/Ho mass ratios in all carbonate phases are similar to the source and unaltered host ratios (27–29), while the apatites have slightly lower ratios of ~24 (Table 4; Genna et al., 2014). Mineralogical control by calcite and apatite (Bea et al., 1994) likely suppressed Y incorporation relative to Ho. Preferential Y complexation by fluorine would result in a Y/Ho increase along the fluid pathway (Fig. 9). There are no indications for a contribution from a F-rich magmatic fluid, but F could have been derived locally from sericite breakdown, and there is evidence for F-rich fluids in the form of fluorapatite (Genna et al., 2014). The lack of anomalously high Y/Ho ratios could reflect Y retention in F-rich parental fluids, in combination with suppression of mineralogical control in a relatively open system.

The inherited Eu/Eu^*_N values from the rhyolitic source area are likely below unity with PAAS as reference composition, while anorthoclase-rich mafic units likely provide higher Eu/Eu^*_N during albitization and sericitization (Fig. 10). Nonetheless, hydrothermal vent fluids are typically characterized by high Eu/Eu^*_N ratios (e.g., Craddock et al., 2010), and this reflects Eu enrichment associated with preferential transport in strong $Eu^{2+}Cl$ complexes (Fig. 10). The expected enrichment is indeed preserved in the pronounced positive Eu anomalies in the ankerites and disseminated calcites, and especially in the Eu^{2+}-selective apatites (Table 4). Mineralogical control by calcite and ankerite explains the lower Eu/Eu^*_N values, especially in combination with coprecipitating apatite. On average, the vein calcites show lower Eu/Eu^*_N values than the unaltered host (Genna et al., 2014). Furthermore, vein calcites with higher average REEY concentrations tend to have lower Eu/Eu^*_N, while the highest values are restricted to veins with lower REEY content. The latter vein calcites have highly variable Eu/Eu^*_N ratios. Similar tendencies can be observed in the disseminated calcite and ankerite, also when the three cement types are plotted together. This could indicate lower Eu/Eu^*_N in parental fluids with higher $\sum$ REE/Ca or that REEY-rich veins crystallized in more open systems with continuous REEY supply. Alternatively, the higher concentrations could be related to Cl-rich fluids with higher total REEY concentrations, wherein stable Eu(II)Cl complexes diminish the availability of Eu^{2+} during precipitation.

Although hydrothermal vent fluids are typically LREE-enriched (Craddock et al., 2010; Douville et al., 1999), disseminated calcites and ankerites are moderately depleted in LREE (Fig. 12C; La/Sm_N ~0.09–0.15) compared to the unaltered host and the inferred source area (La/Sm_N ~0.4–0.8). Similarly, vein calcites and apatites are weakly LREE depleted. This likely reflects coprecipitation in equilibrium with the strongly LREE-selective allanite. The vein calcites also show a stronger HREE depletion (Dy/Yb_N ~3.4) compared to the unaltered host and source area (Dy/Yb_N ~ 0.8–1.2). The latter could indicate a more open system with a stronger mineralogical control. This is corroborated by a tendency towards higher $\sum$ REE and lower Eu/Eu^*_N values in vein calcites with more pronounced HREE fractionation.

10.5. Multiphase stratiform Cu–Co mineralization at Nkana (≤200–450 °C)

The Central African Copperbelt contains numerous sediment-hosted Cu–Co deposits which experienced multi-stage mineralization (Muchez et al., 2010). This final example intends to demonstrate that superposition of several stages following different pathways with different physicochemical conditions considerably complicates interpretation of REEY signatures.

The Zambian Nkana–Mindola deposit is one of the larger, well-studied deposits in the Central African Copperbelt and is currently mined along a 14 km long transect. Mineralization occurred in multiple phases. The layer parallel veins record supra-lithostatic pressures at the onset of basin inversion during the ~590–530 Ma Lufilian orogeny (Selley et al., 2005). The mineralizing fluids were originally seawater-derived, infiltrating lagoonal brines or crustal fluids re-dissolving evaporate layers; and the fluids likely became less oxidizing at the later mineralization stages (Eglinger et al., 2013). Based on Nd isotope data (Van Wilderode et al., 2015) and the current metallogenetic models, the local basement and the overlying sediments constitute the most likely solid source area. Primary or hydrothermal apatite (<20 μm) of uncertain paragenetic affinity occurs disseminated throughout the host rock (Brems et al., 2009), and could represent an important potential coprecipitating phase at some stages. The earliest mineralization phases occur in nodules, fibrous and non-fibrous layer-parallel dolomite veins At this stage, fluid migration is thought to be dominantly lateral, originating from the deeper parts of the Katanga sedimentary basin, potentially with a contribution from the underlying basement (Muchez et al., 2010). Isotopic evidence indicates that irregular veins reflect remobilization during the Lufilian deformation of previously layer-parallel veins (Brems et al., 2009). Finally, different sets of relatively undeformed cleavage-discordant veins crosscut all earlier mineralization phases. First appearances of anhydrite, carrolite, pentlandite ± molybdenite in these veins indicate that they represent a new fluid input, likely originating from the underlying basement (Muchez et al., 2010). Nonetheless, Nd isotopic compositions of gangue carbonates associated with the mineralization are identical in all mineral phases at Nkana (Van Wilderode et al., 2015). Tremolite and talc porphyroblasts grew syn- to post-kinematic to the cleavage discordant mineralization phases and constrain greenschist facies temperature conditions of ≥400 °C.

Despite precipitating from ligand-rich brines at elevated temperatures, REEY concentrations in the Nkana carbonates are only 5 to 7 times higher than in marine carbonates (e.g., Webb and Kamber, 2000). This can be attributed to significantly higher Ca concentrations in crustal brines (Table 1), which significantly lowers the REE/Ca ratios in the parental fluids. Five main pattern types are distinguished in Table 4 and Fig. 12D: upwards convex patterns in nodule and veins with fibrous dolomites (Type I), ramp-flat to slightly rising patterns in layer parallel veins with blocky dolomites (Type II), log-linear increasing patterns in calcites and dolomites from most cleavage-discordant veins (Type III), a small subset of dolomites from cleavage-discordant veins with log-linear increasing LREE and flat MREE/HREE transects (Type IV) and finally REEY-rich calcites with ramp-flat shaped patterns (Type X).

The HREE enrichment in Type III (Fig. 12D) could in principle be directly inherited from mineral–rock equilibria (Fig. 8). HREE-enriched granites are indeed known in the basement below the Zambian Copperbelt (Katongo et al., 2004). However, there is no empirical evidence for such HREE-enriched fluids originating from fluid–rock equilibria. At the slightly acidic pH expected in NaCl rich mineralizing fluids equilibrating with country rocks (Muchez and Corbella, 2012), the HREE-selective OH^- and CO_3^{2-} are likely not the main REE transporting species. Complexation-driven fractionation therefore also seems unlikely. Nonetheless, preferential LREE retention in Cl (±F) complexes during precipitation likely contributed to the relative HREE enrichment. However, stability constants are similar for all HREE, and therefore, this process does not account for the progressive HREE enrichment. Sorption is expected to preferentially remove HREE, but is less prominent at high temperatures. At the crystallization site, CO_3^{2-} activity is likely high and an incorporation step involving $REECO_3^-$ complexes would likely result in a HREE enrichment. However, this process would always operate for hydrothermal carbonates, while the HREE enrichment is more prominent than in other veins. By elimination, the only processes that could account for the HREE enrichment are remobilization and Rayleigh fractionation of a LREE-selective mineral phase. Interestingly, both calcite and dolomite exhibit Type III patterns, indicating that differences due to mineralogical control between these minerals are limited here. Nonetheless, the Type X calcites that occur as infill in intensely silicified parts of the shale host record the highest REEY concentrations and have high La/Sm_N ratios (0.27). The volumetrically minor equidimensional cleavage-discordant veins lack the distinctive HREE enrichment. Absence of associated ore minerals suggest less pervasive fluid flow compared to the other cleavage-discordant veins. This indicates crystallizing in a system with a more closed nature, in accordance with their positive Eu anomalies and lower REE concentrations.

The earliest mineralization phases, nodules and layer parallel veins with fibrous dolomite textures, are associated with strong positive Eu anomalies (Type I; Fig. 12D). The presence of synkinematic bitumen suggests temperatures in the range of the oil window, thus below 200 °C. The pronounced positive Eu anomalies (Eu/Eu^*_N 2.8) are then directly inherited from the sources. Alternatively, the Eu enrichment could represent a 'fossil' Eu anomaly resulting from preferential complexation of Eu^{2+} by Cl complexes in a high-temperature part of the pathway (cf. Bau et al. (2010)). Conversely, layer-parallel veins with blocky dolomites (Type II) and cleavage-discordant veins (Type III,

>400 °C) display pronounced negative Eu anomalies, unlike the Type IV cleavage-discordant veins (Fig. 12D). The negative Eu anomalies do not preclude parental fluids with pronounced positive Eu anomalies, since Eu^{2+} behaves incompatibly during crystallization and is likely retained in stable Cl complexes at high temperatures in open systems. Additionally, the incompatible, fluid-mobile divalent Eu could be preferentially removed during recrystallization in equilibrium with subsequent fluid pulses. The positive anomalies in a subset of cleavage-discordant veins could be related to a less pronounced open system character (Fig. 7), or lower [REE] in the fluid due to lower Cl activity, as indicated by REE concentrations that are 3 to 4 times lower.

Actual Ce anomalies are restricted to the layer-parallel veins with fibrous texture (Type I), as these are the only carbonates that show elevated Pr/Pr* values (~1.1, Table 4). Remobilization in oxidizing conditions is unlikely to explain the observed Ce anomalies, since the mineralization is hosted in siltstones rich in reducing organic matter. Furthermore, while the mineralizing fluids likely equilibrated with more oxidized layers along the fluid pathway (Hitzman et al., 2010), the tetravalent fraction of Ce, which is preferentially retained in Fe–Mn oxides, was likely small or nonexistent. Assuming ideal open system crystallization in combination with the partition ratios from Tanaka and Kawabe (2006), the carbonate Y/Ho_N ratios correspond to 1.4–1.9 Y/Ho_N in the parental fluids, similar to the oxidizing seawater composition (Bau et al., 1997). The elevated Y/Ho ratios in the fluids could be directly inherited from seawater-derived crustal fluids, result from complexation-driven fractionation by F species or through preferential Ho sorption to Fe–Mn oxyhydroxides (Fig. 9). The relative importance of these processes remains ambiguous.

The REEY signatures in the Nkana dolomites and calcites document a fluid evolution from low-temperature conditions towards greenschist facies conditions. Some dolomites preserved signatures and textures developed early on (Type I), while many dolomites re-equilibrated with subsequent fluids at greenschist conditions (Type II). The distinctive patterns of the most recent, cleavage-discordant calcites and dolomites (Type III) are observed along the entire deposit, and indicate similar physicochemical conditions and processes along the ~14 km long area, except where fluid flow is restricted (Type IV).

11. Conclusions

Carbonate minerals are common gangue minerals in hydrothermal ore deposits, where they incorporate trace amounts of REEY. Since many hydrothermal processes fractionate the REEY, their REEY signatures are widely used as proxies to study ore-forming hydrothermal processes. To track the REEY mass transfer during hydrothermal fluid flow, we adopted a process-centered "source–sink" approach. This approach is visualized in a number of flow charts that summarize the main hydrothermal processes that influence the REEY signatures. Application of this system to four concrete examples illustrates that the source–sink approach allows identifying several permissible explanations for the observed REEY signatures, including superimposed effects. Backtracking the REEY pattern characteristics becomes increasingly difficult when limited constraints from other methods are available or when mineralization occurs in several phases. Nonetheless, the normalized pattern shape, Ce/Ce^*_N and Eu/Eu^*_N anomalies in combination with Y/Ho ratios can provide information about the main hydrothermal processes prior to deposition.

Supplementary data to this article can be found online at http://dx.doi.org/10.1016/j.oregeorev.2015.07.022.

Conflict of interest

The authors declare that there are no conflicts of interest associated with this manuscript.

David Debruyne, Niels Hulsbosch and Philippe Muchez.

Acknowledgments

We are thankful for the suggestions, constructive comments and corrections by D. Genna and an anonymous reviewer. Special thanks to Dr. Tim Horscroft and Editor Pirajno for their keen handling of our manuscript. David Debruyne is a research assistant of the Fund for Scientific Research – Flanders (FWO-Flanders). The research of Niels Hulsbosch is funded by a Ph.D. grant of the Agency for Innovation by Science and Technology (IWT). Additional financial support from the Lu–Hf and Sm–Nd project grant G.A078.11N from FWO Flanders is gratefully acknowledged.

References

Adamo, C., Maldivi, P., 1997. Ionic versus covalent character in lanthanide complexes. A hybrid density functional study. Chem. Phys. Lett. 268, 61–68. http://dx.doi.org/10.1016/S0009-2614(97)00177-2.

Allen, D.E., Seyfried Jr., W.E., 2005. REE controls in ultramafic hosted MOR hydrothermal systems: an experimental study at elevated temperature and pressure. Geochim. Cosmochim. Acta 69, 675–683. http://dx.doi.org/10.1016/j.gca.2004.07.016.

Audétat, A., Günther, D., Heinrich, C.A., 2000. Magmatic–hydrothermal evolution in a fractionating granite: a microchemical study of the sn-w-f-mineralized mole granite (Australia). Geochim. Cosmochim. Acta 64, 3373–3393. http://dx.doi.org/10.1016/S0016-7037(00)00428-2.

Ayers, J., Watson, E., 1991. Solubility of apatite, monazite, zircon, and rutile in supercritical aqueous fluids with implications for subduction zone geochemistry. Philos. Trans. R. Soc. London, Ser. A 335, 365–375. http://dx.doi.org/10.1098/rsta.1991.0052.

Bach, W., Yeats, C.J., Craddock, P.R., Humphris, S.E., Binns, R.A., Roberts, S., Vanko, D.A., 2003. Controls of fluid chemistry and complexation on rare-earth element contents of anhydrite from the Pacmanus subseafloor hydrothermal system, Manus Basin, Papua New Guinea. Miner. Deposita 38, 916–935. http://dx.doi.org/10.1007/s00126-002-0325-0.

Banks, D.A., Yardley, B.W.D., Campbell, A.R., Jarvis, K.E., 1994. REE composition of an aqueous magmatic fluid: a fluid inclusion study from the Capitan Pluton, New Mexico, U.S.A. Chem. Geol. 113, 259–272. http://dx.doi.org/10.1016/0009-2541(94)90070-1.

Banks, D.A., Giuliani, G., Yardley, B.W.D., Cheilletz, A., 2000. Emerald mineralisation in Colombia: fluid chemistry and the role of brine mixing. Miner. Deposita 35, 699–713. http://dx.doi.org/10.1007/s001260050273.

Banner, J.L., Hanson, G.N., Meyers, W.J., 1988. Rare earth element and Nd isotopic variations in regionally extensive dolomites from the Burlington-Keokuk Formation (Mississippian); implications for REE mobility during carbonate diagenesis. J. Sediment. Res. 58, 415–432. http://dx.doi.org/10.1306/212F8DAA-2B24-11D7-8648000102C1865D.

Barker, S.L.l., Cox, S.F., 2011. Oscillatory zoning and trace element incorporation in hydrothermal minerals: insights from calcite growth experiments. Geofluids 11, 48–56. http://dx.doi.org/10.1111/j.1468-8123.2010.00305.x.

Barker, S.L.L., Bennett, V.C., Cox, S.F., Norman, M.D., Gagan, M.K., 2009. Sm–Nd, Sr, C and O isotope systematics in hydrothermal calcite–fluorite veins: implications for fluid–rock reaction and geochronology. Chem. Geol. 268, 58–66. http://dx.doi.org/10.1016/j.chemgeo.2009.07.009.

Bau, M., 1991. Rare-earth element mobility during hydrothermal and metamorphic fluid–rock interaction and the significance of the oxidation state of europium. Chem. Geol. 93, 219–230. http://dx.doi.org/10.1016/0009-2541(91)90115-8.

Bau, M., Dulski, P., 1995. Comparative study of yttrium and rare-earth element behaviours in fluorine-rich hydrothermal fluids. Contrib. Mineral. Petrol. 119, 213–223. http://dx.doi.org/10.1007/BF00307282.

Bau, M., Dulski, P., 1996. Distribution of yttrium and rare-earth elements in the Penge and Kuruman iron-formations, Transvaal Supergroup, South Africa. Precambrian Res. 79, 37–55. http://dx.doi.org/10.1016/0301-9268(95)00087-9.

Bau, M., Dulski, P., 1999. Comparing yttrium and rare earths in hydrothermal fluids from the Mid-Atlantic Ridge: implications for Y and REE behaviour during near-vent mixing and for the Y/Ho ratio of Proterozoic seawater. Chem. Geol. 155, 77–90. http://dx.doi.org/10.1016/S0009-2541(98)00142-9.

Bau, M., Koschinsky, A., 2009. Oxidative scavenging of cerium on hydrous Fe oxide: evidence from the distribution of rare earth elements and yttrium between Fe oxides and Mn oxides in hydrogenetic ferromanganese crusts. Geochem. J. 43, 37–47.

Bau, M., Möller, P., 1992. Rare earth element fractionation in metamorphogenic hydrothermal calcite, magnesite and siderite. Mineral. Petrol. 45, 231–246. http://dx.doi.org/10.1007/BF01163114.

Bau, M., Koschinsky, A., Dulski, P., Hein, J.R., 1996. Comparison of the partitioning behaviours of yttrium, rare earth elements, and titanium between hydrogenetic marine ferromanganese crusts and seawater. Geochim. Cosmochim. Acta 60, 1709–1725. http://dx.doi.org/10.1016/0016-7037(96)00063-4.

Bau, M., Möller, P., Dulski, P., 1997. Yttrium and lanthanides in eastern Mediterranean seawater and their fractionation during redox-cycling. Mar. Chem. 56, 123–131. http://dx.doi.org/10.1016/S0304-4203(96)00091-6.

Bau, M., Balan, S., Schmidt, K., Koschinsky, A., 2010. Rare earth elements in mussel shells of the Mytilidae family as tracers for hidden and fossil high-temperature hydrothermal systems. Earth Planet. Sci. Lett. 299, 310–316. http://dx.doi.org/10.1016/j.epsl.2010.09.011.

Bea, F., Pereira, M.D., Stroh, A., 1994. Mineral/leucosome trace-element partitioning in a peraluminous migmatite (a laser ablation-ICP-MS study). Chem. Geol. 117, 291–312. http://dx.doi.org/10.1016/0009-2541(94)90133-3.

Bodnar, R.J., Reynolds, T.J., Kuehn, C.A., 1985. Fluid inclusion systematics in epithermal systems. In: Berger, B.R., Bethke, P.M. (Eds.), Geology and Geochemistry of Epithermal Systems, Reviews in Economic Geology, pp. 73–98.

Bottrell, S., Yardley, B., 1988. The composition of a primary granite-derived ore fluid from SW England, determined by fluid inclusion analysis. Geochim. Cosmochim. Acta 52, 585–588. http://dx.doi.org/10.1016/0016-7037(88)90114-7.

Brems, D., Muchez, P., Sikazwe, O., Mukumba, W., 2009. Metallogenesis of the Nkana copper–cobalt South Orebody, Zambia. J. Afr. Earth Sci. 55, 185–196. http://dx.doi.org/10.1016/j.jafrearsci.2009.04.003.

Busenberg, E., Plummer, L.N., 1985. Kinetic and thermodynamic factors controlling the distribution of SO4 2- and Na+ in calcites and selected aragonites. Geochim. Cosmochim. Acta 49, 713–725.

Byrne, Robert H., Kim, Ki-Hyun, 1990. Rare earth element scavenging in seawater. Geochim. Cosmochim. Acta 54, 2645–2656. http://dx.doi.org/10.1016/0016-7037(90)90002-3.

Byrne, R.H., Kim, K.-H., 1993. Rare earth precipitation and coprecipitation behavior: the limiting role of PO43− on dissolved rare earth concentrations in seawater. Geochim. Cosmochim. Acta 57, 519–526. http://dx.doi.org/10.1016/0016-7037(93)90364-3.

Carpenter, A.B., Trout, M.L., Pickett, E.E., 1974. Preliminary report on the origin and chemical evolution of lead-and zinc-rich oil field brines in central Mississippi. Econ. Geol. 69, 1191–1206. http://dx.doi.org/10.2113/gsecongeo.69.8.1191.

Cetiner, Z.S., Wood, S.A., Gammons, C.H., 2005. The aqueous geochemistry of the rare earth elements. Part XIV. The solubility of rare earth element phosphates from 23 to 150 °C. Chem. Geol. 217, 147–169. http://dx.doi.org/10.1016/j.chemgeo.2005.01.001.

Chernov, A.A., 1980. Crystallization processes. Modern CrystallographyCrystal Formation vol. 3. Nauka, Moskow, pp. 7–232.

Craddock, P.R., Bach, W., Seewald, J.S., Rouxel, O.J., Reeves, E., Tivey, M.K., 2010. Rare earth element abundances in hydrothermal fluids from the Manus Basin, Papua New Guinea: indicators of sub-seafloor hydrothermal processes in back-arc basins. Geochim. Cosmochim. Acta 74, 5494–5513. http://dx.doi.org/10.1016/j.gca.2010.07.003.

Curti, E., Kulik, D.A., Tits, J., 2005. Solid solutions of trace Eu(III) in calcite: thermodynamic evaluation of experimental data over a wide range of pH and pCO_2. Geochim. Cosmochim. Acta 69, 1721–1737. http://dx.doi.org/10.1016/j.gca.2004.06.027.

Dawson, J.B., Hinton, R.W., 2003. Trace-element content and partitioning in calcite, dolomite and apatite in carbonatite, Phalaborwa, South Africa. Mineral. Mag. 67, 921–930. http://dx.doi.org/10.1180/0026461036750151.

De Baar, H.J.W., Bacon, M.P., Brewer, P.G., Bruland, K.W., 1985. Rare earth elements in the Pacific and Atlantic Oceans. Geochim. Cosmochim. Acta 49, 1943–1959. http://dx.doi.org/10.1016/0016-7037(85)90089-4.

Debruyne, D., Balcaen, L., Vanhaecke, F., Muchez, P., 2013. REEY characteristics in hydrothermal gangue carbonates within the sediment-hosted Nkana–Mindola Cu–Co deposit (Zambia) and in two polymetallic veintype deposits (Kipushi and Dikulushi, Democratic Republic of Congo). Mineral Deposit Research for a High-Tech World. Presented at the 12th Biennial SGA Meeting edition:, Uppsala, Sweden, pp. 1251–1254.

Diamond, L.W., 2003. Introduction to gas-bearing, aqueous fluid inclusions. In: Samson, I., Anderson, A., Marshall, D. (Eds.), Fluid Inclusions: Analysis and Interpretation. Short Course vol. 32. Mineralogical Association of Canada, pp. 101–158.

Doerner, H.A., Hoskins, W.M., 1925. Coprecipitation of radium and barium sulphates. J. Am. Chem. Soc. 47, 662–675.

Douville, E., Bienvenu, P., Charlou, J.L., Donval, J.P., Fouquet, Y., Appriou, P., Gamo, T., 1999. Yttrium and rare earth elements in fluids from various deep-sea hydrothermal systems. Geochim. Cosmochim. Acta 63, 627–643. http://dx.doi.org/10.1016/S0016-7037(99)00024-1.

Eglinger, A., André-Mayer, A., Vanderhaeghe, O., Mercadier, J., Cuney, M., Decrée, S., Feybesse, J.-L., Milesi, J.-P., 2013. Geochemical signatures of uranium oxides in the Lufilian Belt: from unconformity-related to syn-metamorphic uranium deposits during the Pan-African Orogenic Cycle. Ore Geol. Rev. 54, 197–213. http://dx.doi.org/10.1016/j.oregeorev.2013.04.003.

Elzinga, E.J., Reeder, R.J., Withers, S.H., Peale, R.E., Mason, R.A., Beck, K.M., Hess, W.P., 2002. EXAFS study of rare-earth element coordination in calcite. Geochim. Cosmochim. Acta 66, 2875–2885. http://dx.doi.org/10.1016/S0016-7037(02)00888-8.

Eugster, H.P., 1981. Metamorphic solutions and reactions. Phys. Chem. Earth 13 (14), 461–507. http://dx.doi.org/10.1016/0079-1946(81)90023-9.

Eugster, H., Gunter, W., 1981. The compositions of supercritical metamorphic solutions. Bull. Mineral. 104, 817–826.

Gammons, C., 1996. The aqueous geochemistry of the rare earth elements and yttrium: VI. Stability of neodymium chloride complexes from 25 to 300 °C. Geochim. Cosmochim. Acta 60, 4615–4630. http://dx.doi.org/10.1016/S0016-7037(96)00262-1.

Genna, D., Gaboury, D., Roy, G., 2014. Evolution of a volcanogenic hydrothermal system recorded by the behavior of LREE and Eu: case study of the Key Tuffite at Bracemac–McLeod deposits, Matagami, Canada. Ore Geol. Rev. 63, 160–177. http://dx.doi.org/10.1016/j.oregeorev.2014.04.019.

Gibert, F., Montel, J.-M., 1996. Étude expérimentale de la solubilité de la monazite dans des fluides à H2O–CO2. Presented at the Réunion des Sciences de la Terre, Orléans.

Göb, S., Loges, A., Nolde, N., Bau, M., Jacob, D.E., Markl, G., 2013. Major and trace element compositions (including REE) of mineral, thermal, mine and surface waters in SW Germany and implications for water–rock interaction. Appl. Geochem. 33, 127–152. http://dx.doi.org/10.1016/j.apgeochem.2013.02.006.

Gromet, L.P., Haskin, L.A., Korotev, R.L., Dymek, R.F., 1984. The "North American shale composite": its compilation, major and trace element characteristics. Geochim. Cosmochim. Acta 48, 2469–2482. http://dx.doi.org/10.1016/0016-7037(84)90298-9.

Haas, J.R., Shock, E.L., Sassani, D.C., 1995. Rare earth elements in hydrothermal systems: estimates of standard partial molal thermodynamic properties of aqueous complexes of the rare earth elements at high pressures and temperatures. Geochim. Cosmochim. Acta 59, 4329–4350. http://dx.doi.org/10.1016/0016-7037(95)00314-P.

Haest, M., Muchez, P., Dewaele, S., Boyce, A.J., von Quadt, A., Schneider, J., 2009. Petrographic, fluid inclusion and isotopic study of the Dikulushi Cu–Ag deposit, Katanga (D.R.C.): implications for exploration. Miner. Deposita 44, 505–522. http://dx.doi.org/10.1007/s00126-009-0230-x.

Haest, M., Schneider, J., Cloquet, C., Latruwe, K., Vanhaecke, F., Muchez, P., 2010. Pb isotopic constraints on the formation of the Dikulushi Cu–Pb–Zn–Ag mineralisation, Kundelungu Plateau (Democratic Republic of Congo). Miner. Deposita 45, 393–410. http://dx.doi.org/10.1007/s00126-010-0279-6.

Hanor, J.S., 1994. Origins of saline fluids in sedimentary basins. Geol. Soc. Lond. Spec. Publ. 151–174.

Hecht, L., Freiberger, R., Gilg, H.A., Grundmann, G., Kostitsyn, Y.A., 1999. Rare earth element and isotope (C, O, Sr) characteristics of hydrothermal carbonates: genetic implications for dolomite-hosted talc mineralization at Göpfersgrün (Fichtelgebirge, Germany). Chem. Geol. 155, 115–130. http://dx.doi.org/10.1016/S0009-2541(98)00144-2.

Heijlen, W., Muchez, P., Banks, D.A., 2001. Origin and evolution of high-salinity, Zn–Pb mineralising fluids in the Variscides of Belgium. 36, 165–176. http://dx.doi.org/10.1007/s001260050296.

Henjes-Kunst, F., Prochaska, W., Niedermayr, A., Sullivan, N., Baxter, E., 2014. Sm–Nd dating of hydrothermal carbonate formation: an example from the Breitenau magnesite deposit (Styria, Austria). Chem. Geol. 387, 184–201. http://dx.doi.org/10.1016/j.chemgeo.2014.07.025.

Hitzman, M.W., Selley, D., Bull, S., 2010. Formation of sedimentary rock-hosted stratiform copper deposits through earth history. Econ. Geol. 105, 627–639. http://dx.doi.org/10.2113/gsecongeo.105.3.627.

Holland, H.D., 2006. The oxygenation of the atmosphere and oceans. Philos. Trans. R. Soc. B Biol. Sci. 361, 903–915. http://dx.doi.org/10.1098/rstb.2006.1838.

Hughes, J., Cameron, M., Crowley, K., 1989. Structural variations in natural F, OH, and Cl apatites. Am. Mineral. 74, 870–876.

James, R.H., Green, D.R.H., Stock, M.J., Alker, B.J., Banerjee, N.R., Cole, C., German, C.R., Huvenne, V.A.I., Powell, A.M., Connelly, D.P., 2014. Composition of hydrothermal fluids and mineralogy of associated chimney material on the East Scotia Ridge back-arc spreading centre. Geochim. Cosmochim. Acta 139, 47–71. http://dx.doi.org/10.1016/j.gca.2014.04.024.

Jordan, D.S., Saslow, S.A., Geiger, F.M., 2011. Exponential sensitivity and speciation of Al(III), Sc(III), Y(III), La(III), and Gd(III) at fused silica/water interfaces. J. Phys. Chem. A 115, 14438–14445. http://dx.doi.org/10.1021/jp208843v.

Kamber, B.S., Webb, G.E., 2001. The geochemistry of late Archaean microbial carbonate: implications for ocean chemistry and continental erosion history. Geochim. Cosmochim. Acta 65, 2509–2525. http://dx.doi.org/10.1016/S0016-7037(01)00613-5.

Kamber, B.S., Greig, A., Collerson, K.D., 2005. A new estimate for the composition of weathered young upper continental crust from alluvial sediments, Queensland, Australia. Geochim. Cosmochim. Acta 69, 1041–1058. http://dx.doi.org/10.1016/j.gca.2004.08.020.

Katongo, C., Koller, F., Kloetzli, U., Koeberl, C., Tembo, F., De Waele, B., 2004. Petrography, geochemistry, and geochronology of granitoid rocks in the Neoproterozoic–Paleozoic Lufilian–Zambezi belt, Zambia: implications for tectonic setting and regional correlation. J. Afr. Earth Sci. 40, 219–244. http://dx.doi.org/10.1016/j.jafrearsci.2004.12.007.

Kontak, D.J., Jackson, S., 1995. Laser-ablation ICP-MS microanalysis of calcite cement from a Mississippi-Valley-type Zn–Pb deposit, Nova-Scotia — dramatic variability in REE content on macro-scales and micro-scales. Can. Mineral. 33, 445–467.

Kontak, D.J., Jackson, S.J., 1999. Documentation of variable trace- and rare-earth-element abundances in carbonates from auriferous quartz veins in meguma lode-gold deposits, Nova Scotia. Can. Mineral. 37, 469–488.

Kučera, J., Cempírek, J., Dolníček, Z., Muchez, P., Prochaska, W., 2009. Rare earth elements and yttrium geochemistry of dolomite from post-Variscan vein-type mineralization of the Nízký Jeseník and Upper Silesian Basins, Czech Republic. J. Geochem. Explor. 103, 69–79. http://dx.doi.org/10.1016/j.gexplo.2009.08.001.

Lakshtanov, L.Z., Stipp, S.L.S., 2004. Experimental study of europium (III) coprecipitation with calcite. Geochim. Cosmochim. Acta 68, 819–827. http://dx.doi.org/10.1016/j.gca.2003.07.010.

Land, L.S., Macpherson, G.L., 1992. Origin of saline formation waters, cenozoic section, Gulf of Mexico Sedimentary Basin (1). AAPG Bull. 76, 1344–1362.

Lee, J.H., Byrne, R.H., 1992. Examination of comparative rare earth element complexation behavior using linear free-energy relationships. Geochim. Cosmochim. Acta 56, 1127–1137. http://dx.doi.org/10.1016/0016-7037(92)90050-S.

Lüders, V., Möller, P., Dulski, P., 1993. REE fractionation in carbonates and fluorites. In: Moeller, P., Lüders, V. (Eds.), Formation of Hydrothermal Vein DepositsMonograph Series on Mineral Deposits. Gebrüter Borntraeger, Berlin, pp. 133–150.

Mahood, G., Hildreth, W., 1983. Large partition coefficients for trace elements in high-silica rhyolites. Geochim. Cosmochim. Acta 47, 11–30. http://dx.doi.org/10.1016/0016-7037(83)90087-X.

Malone, M.J., Baker, P.A., 1999. Temperature dependence of the strontium distribution coefficient in calcite: an experimental study from 40° to 200 °C and application to natural diagenetic calcites. J. Sediment. Res. 69.

Maskenskaya, O.M., Drake, H., Mathurin, F.A., Åström, M.E., 2015. The role of carbonate complexes and crystal habit on rare earth element uptake in low-temperature calcite in fractured crystalline rock. Chem. Geol. 391, 100–110. http://dx.doi.org/10.1016/j.chemgeo.2014.10.030.

Mathurin, F.A., Åström, M.E., Drake, H., Maskenskaya, O.M., Kalinowski, B.E., 2014. REE and Y in groundwater in the upper 1.2 km of Proterozoic granitoids (Eastern Sweden) — assessing the role of composition and origin of groundwaters, geochemistry of fractures, and organic/inorganic aqueous complexation. Geochim. Cosmochim. Acta 144, 342–378. http://dx.doi.org/10.1016/j.gca.2014.08.004.

Matsui, M., 1966. The coprecipitation behaviour of rare earth elements with calcium oxalate upon precipitation from homogeneous systems. Bull. Chem. Soc. Jpn. 39, 1114–1119.

Mayanovic, R.A., Anderson, A.J., Bassett, W.A., Chou, I.-M., 2009. The structure and stability of aqueous rare-earth elements in hydrothermal fluids: New results on neodymium(III) aqua and chloroaqua complexes in aqueous solutions to 500 °C and 520 MPa. Chem. Geol., Experimental Techniques for the Study of Hydrothermal Fluids and Silicate Melts 259, pp. 30–38. http://dx.doi.org/10.1016/j.chemgeo.2008.08.011.

Mccaffrey, M., Lazar, B., Holland, H., 1987. The evaporation path of seawater and the coprecipitation of Br− and K+ with halite. J. Sediment. Petrol. 57, 928–937.

McCaig, A.M., Tritlla, J., Banks, D.A., 2000. Fluid mixing and recycling during Pyrenean thrusting: evidence from fluid inclusion halogen ratios. Geochim. Cosmochim. Acta 64, 3395–3412. http://dx.doi.org/10.1016/S0016-7037(00)00437-3.

Migdisov, A.A., Williams-Jones, A.E., 2002. A spectrophotometric study of neodymium(III) complexation in chloride solutions. Geochim. Cosmochim. Acta 66, 4311–4323. http://dx.doi.org/10.1016/S0016-7037(02)00995-X.

Migdisov, A.A., Williams-Jones, A.E., 2007. An experimental study of the solubility and speciation of neodymium (III) fluoride in F-bearing aqueous solutions. Geochim. Cosmochim. Acta 71, 3056–3069. http://dx.doi.org/10.1016/j.gca.2007.04.004.

Migdisov, A.A., Williams-Jones, A.E., 2014. Hydrothermal transport and deposition of the rare earth elements by fluorine-bearing aqueous liquids. Miner. Deposita 49, 987–997. http://dx.doi.org/10.1007/s00126-014-0554-z.

Migdisov, A.A., Williams-Jones, A.E., Normand, C., Wood, S.A., 2008. A spectrophotometric study of samarium (III) speciation in chloride solutions at elevated temperatures. Geochim. Cosmochim. Acta 72, 1611–1625. http://dx.doi.org/10.1016/j.gca.2008.01.007.

Migdisov, A.A., Williams-Jones, A.E., Wagner, T., 2009. An experimental study of the solubility and speciation of the Rare Earth Elements (III) in fluoride- and chloride-bearing aqueous solutions at temperatures up to 300 °C. Geochim. Cosmochim. Acta 73, 7087–7109. http://dx.doi.org/10.1016/j.gca.2009.08.023.

Millero, F.J., 1992. Stability constants for the formation of rare earth-inorganic complexes as a function of ionic strength. Geochim. Cosmochim. Acta 56, 3123–3132. http://dx.doi.org/10.1016/0016-7037(92)90293-R.

Moffett, J.W., 1990. Microbially mediated cerium oxidation in sea water. Nature 345, 421–423. http://dx.doi.org/10.1038/345421a0.

Möller, P., 1997. Rare earth element and yttrium fractionation caused by fluid migration. J. Geosci. 42, 43-43.

Möller, P., 2002. Rare earth elements and yttrium in geothermal fluids. In: Stober, I.B (Ed.)Water Science and Technology Library 40, 97–125.

Möller, P., Giese, U., 1997. Determination of easily accessible metal fractions in rocks by batch leaching with acid cation-exchange resin. Chem. Geol. 137, 41–55. http://dx.doi.org/10.1016/S0009-2541(96)00149-0.

Möller, P., Lüders, V., Schröder, J., Luck, J., 1991. Element partitioning in calcite as a function of solution flow rate: a study on vein calcites from the Harz Mountains. Miner. Deposita 26. http://dx.doi.org/10.1007/BF00209255.

Möller, P., Irber, W., Giese, U., 1997a. Element mobility in paragneisses and metabasites of the Continental Deep Drilling Project (KTB/Germany). Geol. Rundsch. 86, S184–S198. http://dx.doi.org/10.1007/PL00014653.

Möller, P., Stober, I., Dulski, P., 1997b. Seltenerdelement-, Yttrium-Gehalte und Bleiisotope in Thermal- und Mineralwässern des Schwarzwaldes. Grundwasser 2, 118–132. http://dx.doi.org/10.1007/s767-1997-8533-0.

Möller, P., Dulski, P., Morteani, G., 2003. Partitioning of rare earth elements, yttrium, and some major elements among source rocks, liquid and vapor of Larderello–Travale geothermal field, Tuscany (Central Italy). Geochim. Cosmochim. Acta 67, 171–183. http://dx.doi.org/10.1016/S0016-7037(02)01054-2.

Möller, P., Dulski, P., Savascin, Y., Conrad, M., 2004. Rare earth elements, yttrium and Pb isotope ratios in thermal spring and well waters of West Anatolia, Turkey: a hydrochemical study of their origin. Chem. Geol. 206, 97–118. http://dx.doi.org/10.1016/j.chemgeo.2004.01.009.

Muchez, P., Corbella, M., 2012. Factors controlling the precipitation of copper and cobalt minerals in sediment-hosted ore deposits: advances and restrictions. J. Geochem. Explor. 118, 38–46. http://dx.doi.org/10.1016/j.gexplo.2012.04.006.

Muchez, P., Brems, D., Clara, E., De Cleyn, A., Lammens, L., Boyce, A., De Muynck, D., Mukumba, W., Sikazwe, O., 2010. Evolution of Cu–Co mineralizing fluids at Nkana Mine, Central African Copperbelt, Zambia. J. Afr. Earth Sci. 58, 457–474. http://dx.doi.org/10.1016/j.jafrearsci.2010.05.003.

Munz, I.A., Yardley, B.W.D., Banks, D.A., Wayne, D., 1995. Deep penetration of sedimentary fluids in basement rocks from southern Norway: evidence from hydrocarbon and brine inclusions in quartz veins. Geochim. Cosmochim. Acta 59, 239–254. http://dx.doi.org/10.1016/0016-7037(94)00322-D.

Oberthür, T., Melcher, F., Henjes-Kunst, F., Gerdes, A., Stein, H., Zimmerman, A., El Ghorfi, M., 2009. Hercynian age of the cobalt–nickel–arsenide–(gold) ores, Bou Azzer, Anti-Atlas, Morocco: Re–Os, Sm–ND and U–Pb age determinations. Econ. Geol. 104, 1065–1079. http://dx.doi.org/10.2113/gsecongeo.104.7.1065.

Ohr, M., Halliday, A.N., Peacor, D.R., 1994. Mobility and fractionation of rare earth elements in argillaceous sediments: implications for dating diagenesis and low-grade metamorphism. Geochim. Cosmochim. Acta 58, 289–312. http://dx.doi.org/10.1016/0016-7037(94)90465-0.

Pearson, R.G., 1963. Hard and soft acids and bases. J. Am. Chem. Soc. 85, 3533–3539. http://dx.doi.org/10.1021/ja00905a001.

Petford, N., Cruden, A.R., McCaffrey, K.J.W., Vigneresse, J.-L., 2000. Granite magma formation, transport and emplacement in the Earth's crust. Nature 408, 669–673. http://dx.doi.org/10.1038/35047000.

Poitrasson, F., Oelkers, E., Schott, J., Montel, J.-M., 2004. Experimental determination of synthetic NdPO4 monazite end-member solubility in water from 21 °C to 300 °C: implications for rare earth element mobility in crustal fluids. Geochim. Cosmochim. Acta 68, 2207–2221. http://dx.doi.org/10.1016/j.gca.2003.12.010.

Pourmand, A., Dauphas, N., Ireland, T.J., 2012. A novel extraction chromatography and MC-ICP-MS technique for rapid analysis of REE, Sc and Y: revising CI-chondrite and Post-Archean Australian Shale (PAAS) abundances. Chem. Geol. 291, 38–54. http://dx.doi.org/10.1016/j.chemgeo.2011.08.011.

Pourtier, E., Devidal, J.-L., Gibert, F., 2010. Solubility measurements of synthetic neodymium monazite as a function of temperature at 2 kbars, and aqueous neodymium speciation in equilibrium with monazite. Geochim. Cosmochim. Acta 74, 1872–1891. http://dx.doi.org/10.1016/j.gca.2009.12.023.

Powell, H.K.P., 1974. Entropy titrations: a reassessment of data for the reaction of the sulphate ion with trivalent lanthanoid ions. J. Chem. Soc. Dalton Trans. 1108–1112.

Quinn, K.A., Byrne, R.H., Schijf, J., 2006a. Sorption of yttrium and rare earth elements by amorphous ferric hydroxide: influence of pH and ionic strength. Mar. Chem., AQUACHEM — 04 Mediterranean Conference on Chemistry of Aquatic Systems, Reggio Calabria, Italy, 4th–8th September 2004 99, pp. 128–150 http://dx.doi.org/10.1016/j.marchem.2005.05.011.

Quinn, K.A., Byrne, R.H., Schijf, J., 2006b. Sorption of yttrium and rare earth elements by amorphous ferric hydroxide: influence of solution complexation with carbonate. Geochim. Cosmochim. Acta 70, 4151–4165. http://dx.doi.org/10.1016/j.gca.2006.06.014.

Rankin, A.H., Ramsey, M.H., 1992. The composition of hypersaline, iron-rich granitic fluids based on laser-ICP and Synchrotron-XRF microprobe analysis of individual fluid inclusions in topaz, Mole granite, eastern Australia. Geochim. Cosmochim. Acta 56, 67–79. http://dx.doi.org/10.1016/0016-7037(92)90117-2.

Reed, M.J., Candela, P.A., Piccoli, P.M., 2000. The distribution of rare earth elements between monzogranitic melt and the aqueous volatile phase in experimental investigations at 800 °C and 200 MPa. Contrib. Mineral. Petrol. 140, 251–262. http://dx.doi.org/10.1007/s004100000182.

Reynolds, R.C., 1978. Polyphenol inhibition of calcite precipitation in Lake Powell. Limnol. Oceanogr. 23, 585–597. http://dx.doi.org/10.4319/lo.1978.23.4.0585.

Roberts, S., Palmer, M.R., Cooper, M.J., Buchaus, P., Sargent, D., 2009. REE and Sr isotope characteristics of carbonate within the Cu–Co mineralized sedimentary sequence of the Nchanga Mine, Zambian Copperbelt. Miner. Deposita 44, 881–891.

Rudnick, R.L., Gao, S., 2003. Composition of the Continental Crust. Treatise on Geochemistry. Elsevier, pp. 1–64.

Schijf, J., Byrne, R.H., 2004. Determination of SO4β1 for yttrium and the rare earth elements at I = 0.66 m and t = 25 °C—implications for YREE solution speciation in sulfate-rich waters. Geochim. Cosmochim. Acta 68, 2825–2837. http://dx.doi.org/10.1016/j.gca.2003.12.003.

Selley, D., Broughton, D., Scott, R.J., Hitzman, M., Bull, S.W., Large, R.R., McGoldrick, P.J., Croaker, M., Pollington, N., 2005. A New Look at the Geology of the Zambian Copperbelt. Soc. Econ. Geol. Inc 100th Anniversary Volume.

Shannon, R.D., 1976. Revised effective ionic radii and systematic studies of interatomic distances in halides and chalcogenides. Acta Crystallogr. Sect. A 32, 751–767. http://dx.doi.org/10.1107/S0567739476001551.

Shibata, S.-N., Tanaka, T., Yamamoto, K., 2006. Crystal structure control of the dissolution of rare earth elements in water–mineral interactions. Geochem. J. 40, 437–446. http://dx.doi.org/10.2343/geochemj.40.437.

Shields, G.A., Webb, G.E., 2004. Has the REE composition of seawater changed over geological time? Chem. Geol. 204, 103–107. http://dx.doi.org/10.1016/j.chemgeo.2003.09.010.

Smith, M.P., Henderson, P., Campbell, L.S., 2000. Fractionation of the REE during hydrothermal processes: constraints from the Bayan Obo Fe–REE–Nb deposit, Inner Mongolia, China. Geochim. Cosmochim. Acta 64, 3141–3160. http://dx.doi.org/10.1016/S0016-7037(00)00416-6.

Spangenberg, J., Fontbote, L., 1995. Rare earth element patterns in the host and gangue carbonates of the San-Vincente zinc–lead deposit, Peru. Schweiz. Mineral. Petrogr. Mitt. 75, 271–275.

Sverjensky, D.A., 1984. Europium redox equilibria in aqueous solution. Earth Planet. Sci. Lett. 67, 70–78. http://dx.doi.org/10.1016/0012-821X(84)90039-6.

Tanaka, K., Kawabe, I., 2006. REE abundances in ancient seawater inferred from marine limestone and experimental REE partition coefficients between calcite and aqueous solution. Geochem. J. 40, 425–435. http://dx.doi.org/10.2343/geochemj.40.425.

Tanaka, K., Ohta, A., Kawabe, I., 2004. Experimental REE partitioning between calcite and aqueous solution at 25 degrees C and 1 atm: constraints on the incorporation of seawater REE into seamount-type limestones. Geochem. J. 38, 19–32.

Tanaka, K., Takahashi, Y., Shimizu, H., 2008. Local structure of Y and Ho in calcite and its relevance to Y fractionation from Ho in partitioning between calcite and aqueous solution. Chem. Geol. 248, 104–113. http://dx.doi.org/10.1016/j.chemgeo.2007.11.003.

Tanaka, K., Takahashi, Y., Shimizu, H., 2009. Determination of the host phase of rare earth elements in natural carbonate using X-ray absorption near-edge structure. Geochem. J. 43, 143–149.

Taylor, S.R., McLennan, S.M., 1985. The Continental Crust: Its Composition and Evolution. Blackwell Science, Oxford.

Terakado, Y., Masuda, A., 1988. The coprecipitation of rare-earth elements with calcite and aragonite. Chem. Geol. 69, 103–110. http://dx.doi.org/10.1016/0009-2541(88)90162-3.

Tertre, E., Hofmann, A., Berger, G., 2008. Rare earth element sorption by basaltic rock: experimental data and modeling results using the "generalised composite approach.". Geochim. Cosmochim. Acta 72, 1043–1056. http://dx.doi.org/10.1016/j.gca.2007.12.015.

Thomas, R., Davidson, P., 2012. Water in granite and pegmatite-forming melts. Ore Geol. Rev. 46, 32–46. http://dx.doi.org/10.1016/j.oregeorev.2012.02.006.

Tropper, P., Manning, C.E., Harlov, D.E., 2011. Solubility of CePO4 monazite and YPO4 xenotime in H2O and H2O–NaCl at 800 °C and 1 GPa: implications for REE and Y transport during high-grade metamorphism. Chem. Geol. 282, 58–66. http://dx.doi.org/10.1016/j.chemgeo.2011.01.009.

Tsay, A., Zajacz, Z., Sanchez-Valle, C., 2014. Efficient mobilization and fractionation of rare-earth elements by aqueous fluids upon slab dehydration. Earth Planet. Sci. Lett. 398, 101–112. http://dx.doi.org/10.1016/j.epsl.2014.04.042.

Tsuno, H., Kagi, H., Akagi, T., 2002. High yield of vaterite precipitation induced by trace lanthanum ion from a supersaturated solution of calcium carbonate at 50 °C. Chem. Lett. 31, 960–961. http://dx.doi.org/10.1246/cl.2002.960.
Turekian, K.K., 1968. Oceans. Prentice-Hall, Englewood, Cliffs, N.J.
Van Sijl, J., Allan, N.L., Davies, G.R., van Westrenen, W., 2009. Molecular modelling of rare earth element complexation in subduction zone fluids. Geochim. Cosmochim. Acta 73, 3934–3947. http://dx.doi.org/10.1016/j.gca.2009.04.001.
Van Wilderode, J., Debruyne, D., Torremans, K., Elburg, M.A., Vanhaecke, F., Muchez, P., 2015. Metal sources for the Nkana and Konkola stratiform Cu–Co deposits (Zambian Copperbelt): insights from Sr and Nd isotope ratios. Ore Geol. Rev. 67, 127–138. http://dx.doi.org/10.1016/j.oregeorev.2014.11.011.
Veksler, I.V., 2004. Liquid immiscibility and its role at the magmatic–hydrothermal transition: a summary of experimental studies. Chem. Geol., The magmatic to Hydrothermal Transition and its Bearing on Ore-forming Processes 210, pp. 7–31. http://dx.doi.org/10.1016/j.chemgeo.2004.06.002.
Verma, M.P., 2003. A thermodynamic assessment of dissociation constant of water. Presented at the Twenty-Eighth Workshop on Geothermal Reservoir Engineering. Stanford University, Stanford.
Wagner, T., Boyce, A.J., Erzinger, J., 2010. Fluid–rock interaction during formation of metamorphic quartz veins: a REE and stable isotope study from the Rhenish Massif, Germany. Am. J. Sci. 310, 645–682. http://dx.doi.org/10.2475/07.2010.04.
Walker, J.B., Choppin, G.R., 1967. Thermodynamic parameters of fluoride complexes of the lanthanides. Adv. Chem. Ser. 71, 127–140.
Wang, Y.F., Xu, H.F., 2001. Prediction of trace metal partitioning between minerals and aqueous solutions: a linear free energy correlation approach. Geochim. Cosmochim. Acta 65, 1529–1543. http://dx.doi.org/10.1016/S0016-7037(01)00551-8.
Wang, L., Hu, W., Wang, X., Cao, J., Chen, Q., 2014. Seawater normalized REE patterns of dolomites in Geshan and Panlongdong sections, China: implications for tracing dolomitization and diagenetic fluids. Mar. Pet. Geol. 56, 63–73. http://dx.doi.org/10.1016/j.marpetgeo.2014.02.018.
Warren, J.K., 2006. Ancient basins and stratigraphic evolution. Evaporites Sediments Resour. Hydrocarb.pp. 287–373.
Webb, G.E., Kamber, B.S., 2000. Rare earth elements in Holocene reefal microbialites: a new shallow seawater proxy. Geochim. Cosmochim. Acta 64, 1557–1565. http://dx.doi.org/10.1016/S0016-7037(99)00400-7.
Williams, A.E., McKibben, M.A., 1989. A brine interface in the Salton Sea Geothermal System, California: fluid geochemical and isotopic characteristics. Geochim. Cosmochim. Acta 53, 1905–1920. http://dx.doi.org/10.1016/0016-7037(89)90312-8.
Williams-Jones, A.E., Migdisov, A.A., Samson, I.M., 2012. Hydrothermal mobilisation of the rare earth elements — a tale of "Ceria" and "Yttria.". Elements 8, 355–360. http://dx.doi.org/10.2113/gselements.8.5.355.
Withers, S.H., Peale, R.E., Schulte, A.F., Braunstein, G., Beck, K.M., Hess, W.P., Reeder, R.J., 2003. Broad distribution of crystal-field environments for Nd3 + in calcite. Phys. Chem. Miner. 30, 440–448. http://dx.doi.org/10.1007/s00269-003-0331-5.
Wood, S.A., 1990a. The aqueous geochemistry of the rare-earth elements and yttrium: 1, Review of available low-temperature data for inorganic complexes and the inorganic REE speciation of natural waters. Chem. Geol. 82, 159–186. http://dx.doi.org/10.1016/0009-2541(90)90080-Q.
Wood, S.A., 1990b. The aqueous geochemistry of the rare-earth elements and yttrium: 2. Theoretical predictions of speciation in hydrothermal solutions to 350 °C at saturation water vapor pressure. Chem. Geol. 88, 99–125. http://dx.doi.org/10.1016/0009-2541(90)90106-H.
Wood, S., 2004. The hydrothermal geochemistry of the Rare Earth Elements. The Gangue 8, 1–7.
Wood, S.A., Ricketts, A., 2000. Allanite-(Ce) From the Eocene Casto granite, Idaho: response to hydrothermal alteration. Can. Mineral. 38, 81–100. http://dx.doi.org/10.2113/gscanmin.38.1.81.
Wood, S.A., Palmer, D.A., Wesolowski, D., Bénézeth, P., 2002. The aqueous geochemistry of the rare earth elements and yttrium. Part XI. The solubility of Nd(OH)3 and hydrolysis of Nd3 + from 30 to 290 °C at saturated water vapor pressure with in-situ pHm measurement. In: Hellman, R., Wood, S.A. (Eds.), Water–Rock Interactions, Ore Deposits, and Environmental Geochemistry: A Tribute to David A. Crerar 7. The Geochemical Society, Special Publication, pp. 229–256.
Yardley, B.W.D., 2013. The Chemical Composition of Metasomatic Fluids in the Crust. Metasomatism and the Chemical Transformation of Rock, Lecture Notes in Earth System Sciences. Springer, Berlin Heidelberg, pp. 17–51.
Yardley, B.W.D., Bodnar, R.J., 2014. Fluids in the Continental Crust. Geochem. Perspect. 3, 1–2.
Yurimoto, H., Duke, E.F., Papike, J.J., Shearer, C.K., 1990. Are discontinuous chondrite-normalized REE patterns in pegmatitic granite systems the results of monazite fractionation? Geochim. Cosmochim. Acta 54, 2141–2145. http://dx.doi.org/10.1016/0016-7037(90)90277-R.
Zhao, Y.-Y., Zheng, Y.-F., 2013. Geochemical constraints on the origin of post-depositional fluids in sedimentary carbonates of the Ediacaran system in South China. Precambrian Res. 224, 341–363. http://dx.doi.org/10.1016/j.precamres.2012.10.014.
Zhong, S., Mucci, A., 1995. Partitioning of rare earth elements (REEs) between calcite and seawater solutions at 25 °C and 1 atm, and high dissolved REE concentrations. Geochim. Cosmochim. Acta 59, 443–453. http://dx.doi.org/10.1016/0016-7037(94)00381-U.